AN INVESTIGATION INTO METHODS OF MODELLING POSITIVE INHOMOGENEOUS-FIELD BREAKDOWN AND DISCHARGE PROCESSES IN SF_6 WITH EMPHASIS ON THE CORONA STABILISATION PHENOMENON.

Sanjeev Bhutt

A dissertation submitted to the Faculty of Engineering, University of the Witwatersrand, Johannesburg, in fulfillment of the requirements for the degree of Master of Science in Engineering.

Degree awarded with distinction on 30 June 1998

Johannesburg, 1998

Declaration

I declare that this dissertation is my own, unaided work. It is being submitted for the degree of Master of Science in Engineering in the University of the Witwatersrand, Johannesburg. It has not been submitted before for any other degree or examination in any other University.

Sanjeev Bhutt

February 1998

Felix qui potuit rerum cognoscere causas **(*Vergil*)**

Abstract

Corona stabilisation is not a well understood phenomenon, consequently a rigorous theoretical description of how the mechanism operates does not exist. Furthermore, postulates on the precise physical processes that occur during corona stabilised breakdown are varied and conflicting. It was thus essential to develop a qualitative theory of how the mechanism operates around which a quantitative model could be constructed. To this aim, a detailed analysis of available modelling methods and empirical data from published works was carried out. This analysis together with additional finite elements modelling done as part of this work, leads to a proposed qualitative model which serves as a basis for a quantitative model developed to simulate corona stabilised breakdown from a fixed particle defect. There is a favourable comparison between the predictions of the model and published measurements, thus imbuing optimism in the proposed method. The problem of measuring the true charge deployed in a discharge is discussed and an experiment is designed to circumvent this problem.

Table Of Contents

List Of Figures

List Of Symbols

The most frequently used symbols are listed here. Those symbols not listed here are defined at the point in the text where they appear.

Ionisation coefficient	α
Attachment coefficient	η
Diffusion coefficient	β
Permittivity	ε
Secondary Ionisation coefficient	γ
Gas Pressure	P, p
Current	I, i
Current Density	J
Time	t
Displacement	x
Charge	q
Voltage	V
Electric Field Strength	E
Mobility	μ
Distribution function of particles in phase-space	f

Chapter 1. Introduction

In this chapter, the background to the study presented in this thesis is set forth. The objectives and scope of the work are also discussed here. The meaning of certain terms that are key to this study, but which do not have strict definitions and therefore could cause ambiguity, are clarified in this chapter. There are as yet no published attempts at quantitatively modelling corona stabilisation in SF_6. Modelling stages of the total breakdown process have been attempted via various approaches which span many disciplines from complex numerical methods to empirical engineering investigations. This work therefore aims to extract all the theoretical and empirical work done to date from these varied sources and collate the information into one body of work from which an informed decision can be made as to the most suitable and beneficial way to model the corona stabilisation phenomenon.

1.1 Significance of Corona Stabilisation

The term corona stabilisation will be more clearly defined later on, here it is suffic ent to describe it as a phenomenon that occurs when slow rising waveforms are applied to non-linear geometries in SF_6; due to the small rate of increase of the applied potential, the slow drifting positive ions formed by the initial discharge are allowed to accumulate in front of the electrode and distort the background field and in so doing affect the development of subsequent discharges and leader formation.

One of the most common types of defect in SF_6 GIS (gas insulated systems) are metallic particles which occur despite meticulous manufacture and assembly of the equipment. These particles cause a local field enhancement which leads to partial discharges and sometimes to breakdown and thus failure of the equipment and an expensive forced outage.

In SF_6 insulated equipment it is desirable to attain an operating pressure that is as high as possible since this reduces the size of the equipment. However, it is difficult to manufacture and assemble such equipment with perfectly smooth surfaces and without some metallic particles [illegible] sent [1]. Surface roughness, particle contamination and protrusions or edges due to incorrect assembly cause nonlinearities and therefore locally enhanced fields. It is therefore of great practical significance to understand the physical processes behind discharges and breakdown under very non-linear fields. Of major importance in determining the reliability of gas insulated equipment are diagnostic tools. Defects in the metal-enclosed equipment are difficult to locate and characterise, and yet this has to be done by external measurements. The pressures at which the GIS operates is within the corona-stabilisation zone, and this is most likely the breakdown mechanism that operates in the case of such particle induced faults. It is thus important to understand the physical mechanism of corona stabilised breakdown as this will aid in diagnostics of the GIS.

Furthermore, in addition to in-service, on-line diagnostics, research is being done in diagnosing a GIS while *off-line* by means of applying *impulse voltages* to the system. If the corona stabilised behaviour of certain defects under impulses of different risetimes is understood, this will provide information on the defect characteristics.
For all waveshapes, in inhomogeneous geometries, negative breakdown voltages are higher than the positive breakdown voltages. Invariably, breakdown occurs on the positive half cycle of the a.c. voltage. Therefore only positive applied stresses are concentrated on in this work.

1.2 Limited Knowledge of SF_6 Discharge Processes

Partial discharge in SF_6 is, as pointed out by Van Brunt [2], "an enormously complex phenomenon that often exhibits chaotic, nonstationary, or fractal type behaviour". The statement is applicable to all discharge processes especially under conditions of strongly inhomogeneous fields.

Discharge and breakdown mechanisms in air have been studied for almost a century, and so these processes in air are well understood. Accurate models are available to quantify and predict discharges and breakdown in air under various field configurations. For example, Gallimberti produced an accurate computer model for streamer development in air as early as in 1972 [3] and also recently developed a model describing quantitatively the entire long air gap spark-breakdown process [4].

The selfsame properties of SF_6 which makes it a better insulator than air, also prevents the established models for air-discharges from being directly applied to discharges in SF_6. The electron-attaching nature of SF_6 significantly modifies its discharge behaviour as compared to air. Furthermore, SF_6 is used in totally enclosed pressurised equipment and discharge behaviour is substantially affected by pressure.

The fundamental mechanisms of breakdown and partial discharges in SF_6, especially at higher pressures and in non-linear fields, have only recently (in the last decade) come to be understood. The leader-precursor theory, which is now accepted as the mechanism responsible for positive impulse breakdown in SF_6, was only formulated in the latter part of the last decade [5]. Partial discharge or corona formation in highly non-linear fields in SF_6 is not clearly understood as yet since researchers, whether approaching the problem through empirical investigation or theoretical modelling, have conflicting opinions as to the details of the physical mechanisms involved.

1.3 Objectives

In a paper on insulator physics, Wintle [7] states that "one difficulty which besets the engineer is that the original information is often scattered widely over many journals in engineering, physics, chemistry, mathematics and materials science." This is especially true in the subject of gas discharge physics and modelling, therefore an important aim of this work was to extract all the theoretical and empirical work done to date from the varied sources and collate the information into one body of work. This work can then serve as a platform for attempting to obtain a self-consistent predictive model for positive discharge in nonuniform gaps in SF_6. The aims of this study were therefore to:

- Investigate all methods of modelling discharge processes and coalesce the fundamentals into one body of work.
- Analyse modelling methods in terms of their usefulness in providing a greater understanding of corona stabilised discharges.
- Collate empirical data obtained to date and provide an analysis of this information to be able to select the most plausible theories from the various (often contradictory) ones presented.

- Make use of the data obtained from theoretical models and empirical investigations to present a detailed qualitative theory of the physics of the inhomogeneous field discharge processes.
- Present the most feasible approach to be taken to meet the objective of obtaining a quantitative model for corona stabilised discharges and identify what future work is most crucial to obtaining such a model.

1.4 Terminology Clarification

The term *corona stabilisation* is sometimes used synonymously with the terms *space charge effects* or *ion drift* effects. However, all these terms often refer to different phenomena (or to different stages of a discharge phenomenon).

1.4.1 Space Charge

In the most general context, space charge refers to *any or all* of the *three charged particle species* that may exist in the interelectrode space in an SF_6 insulated vessel; and thereby modifying the applied Laplacian electric field in some way.

The term space-charge is also often used to describe the charge at the tip of a streamer filament which controls the growth of the filament - specifically, in theoretical modelling of corona the effect of space charge production during the discharge growth and its effect on the Laplacian electric field is taken into account by means of simultaneous solution of the continuity equations for electrons and ions and the Poisson equation for electric field strength.

1.4.2 Ion Drift

Within the context of the formation of a leader precursor (described in Chapter 2) ion drift refers to the process whereby positive and negative ions formed at the end of a streamer filament drift apart and cause a local field enhancement which may cause a re-start of avalanche activity.

As described by Van Der Zel [8,11], ion drift may also refer to the phenomenon which occurs when the voltage applied to the geometry is not high enough to result in a seed electron being detached from a negative ion. In this case, the negative ions are allowed to drift out of the high stress region near the positive electrode. In the case of a positive voltage being applied to the electrode, the primary source of avalanche-initiating electrons is field induced detachment [5]. A discharge might therefore not occur due to the lack of the initiating electron. This is also sometimes referred to as the "*sweep-field effect.*"

1.4.3 Corona Stabilisation

Corona stabilisation refers to the specific phenomenon whereby positive ions created by a partial discharge are allowed to accumulate around the point electrode due to a slowly rising applied voltage (positive polarity). This accumulated positive charge decreases the electric field strength at the point. The inception of a leader will consequently occur at a higher voltage.

1.4.4 Partial Discharge

A partial discharge may be streamer corona that does not produce a leader or it may happen that a leader forms, but is extinguished before arriving at the opposite electrode. In this work, a partial discharge is considered to be any type of localised discharge that does not result in a complete electrical breakdown [9], and thus electron avalanche activity is also included under this definition as well as the larger streamer discharges. The extinguished leader will not be considered as a partial discharge since leader propagation will not be modelled. In the model therefore, a partial discharge will be deemed to have occurred if a leader precursor fails to form. This fits in with the general categorisation of partial discharges as "cold" discharges where the mean electron energies greatly exceed the mean energies of the gas molecules (heavy particles) [9]. The formation of the precursor leads to heating, nullifying the cold discharge assumption.

Further nomenclature definitions will be made when appropriate.

1.5 Modelling Methodology

It is clear that a discharge process in gas insulated equipment may be categorised as a complex dynamical system. The modelling of such systems often follows a similar set of stages. The general stages to be followed when modelling dynamical systems are as follows [10]:

- Define the scope and accuracy of desired model.
- Obtain a framework of theoretically based equations that (as far as possible) cover all aspects of first-order importance.
- If necessary, supplement the framework obtained above by equations based on experiment and observation.
- Manipulate framework of equations into a form suitable for computer solution.
- Plan and carry out a data acquisition exercise.
- Determine unknown parameters in model.
- Validate model by obtaining further data.

Except for the simplest of models, these steps will be iterated many times before the criteria set down in the first step are fulfilled.

The most essential part of the model building process is to assemble equations that represent the physical mechanisms that are believed to be applicable. Often, the different types of equations available are incompatible - the equations representing the basic processes might be complex, based on complex physics theory, giving rise to many internal relations with unknown and inaccessible parameters. On the other extreme, semi-empirical relationships might be available which have much fewer variables but have a limited accuracy and range of applicability.

This thesis concentrates mainly on the second stage of the modelling process. However, the second stage depends on a clear description of the first stage, which poses the question : What processes need to be modelled ?

Breakdown consists of a number of sub-processes, which are themselves understood to varying degrees. In positive, inhomogeneous field conditions the main subprocesses are:

- Initiatory electron availability.
- Initial avalanche activity and the transition of avalanches to streamers.
- Spatio-temporal streamer growth.
- Transition from streamer to leader.
- Leader propagation, subsequent streamer-leader spatio-temporal development.
- Finally breakdown-arc formation.

We are primarily concerned with the effect the *space charge* deposited by the *initial streamer* corona has on subsequent streamer/leader development. The focus of the modelling in this thesis is consequently on streamers and the formation of the first leader precursor as shown in *Figure 1.1* below. Reference will be made to published work where attempted models of the leader stepping process may be found.

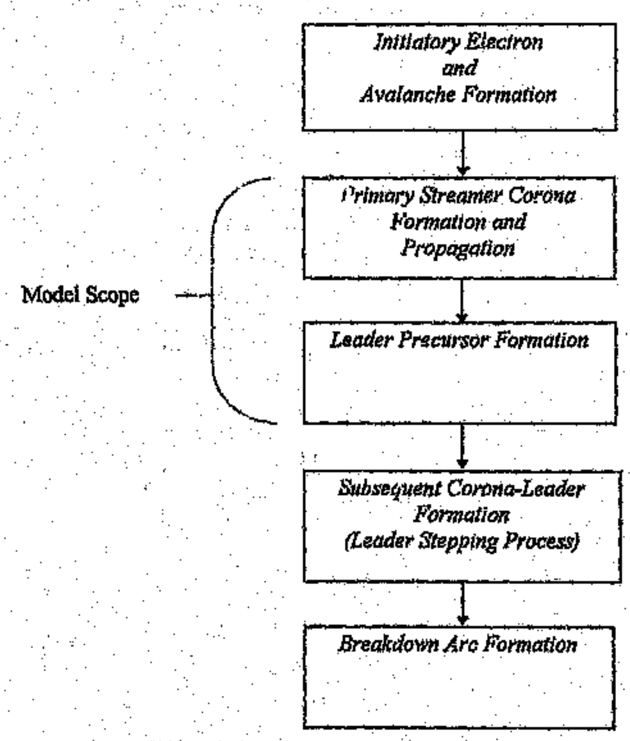

Figure 1.1 Stages of breakdown and scope of model

Furthermore, partial discharge modelling is also of great interest. The term partial discharge as used in this work is defined in 1.4.4 above. In light of this definition, partial discharge modelling is a subset of the model for streamer formation.

Chapter 2. Current Understanding of Inhomogeneous-Field Breakdown in SF_6 without Corona Stabilisation

In the previous chapter, the issues germane to the modelling of breakdown phenomena were introduced, the stages of breakdown were listed and the scope of this work defined in terms of these breakdown stages. The mechanisms mentioned in Chapter 1 will be described in more detail here. This chapter deals with the current knowledge of breakdown in SF_6 under fast rising waveforms where stabilisation by positive ion drift does not occur. The breakdown process under slow rising waveforms in non-linear field situations, which are the conditions under which corona stabilisation occurs, will be described in Chapter 5.

2.1 Relevance of Breakdown without Ion Drift Effects

In order to understand corona stabilised breakdown, it is essential to understand the stabilisation-free mechanism under fast rising impulses, since most physical processes that occur in the latter case must take place under slow-rising voltages as well.

The most recent state of understanding of the mechanism of breakdown in electronegative gases in non-uniform fields and under fast-rising voltage waveforms is discussed here. The theory discussed below was mainly developed by Wiegart et al [5,13,14,15,16], Niemeyer et al [17] and Pinnekamp et al [18,19,20].

2.2 Breakdown via the Leader-Precursor mechanism

In SF_6, under the conditions just mentioned, breakdown will occur via a mechanism called *leader breakdown* for pressures greater than about half an atmosphere. At very low pressures, breakdown will occur via the normal streamer mechanism. Also, it must be emphasised that the mechanisms described in this section apply to non-linear electric fields where the field enhancement factors are typically greater than 1,5

(i.e. $\frac{E_{maximum}}{E_{average}} > 1,5$).

Leader breakdown occurs via a sequence of physical processes. These will be discussed with the aid of *Figure 2.1* below, where they are schematically represented.

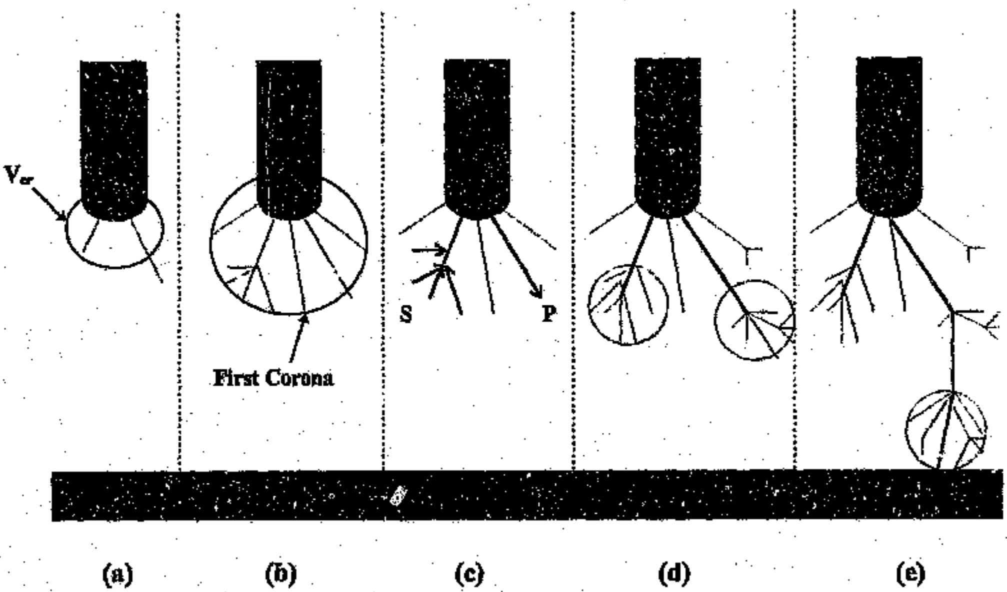

Figure 2.1 : Stepped Leader Breakdown

There are two mechanisms which are responsible for leader formation, the **Stem** mechanism and the **Leader Precursor** mechanism. The Precursor mechanism has greater significance since it is the *only* mechanism present under positive breakdown (i.e. the point is positive with respect to the plane) and is the *predominant* one under negative breakdown.

As the voltage applied to the point increases, a region develops around the electrode where the electric field strength within this region exceeds the critical electric field strength for SF_6 , E_{cr} (which is about 89 kV/mm MPa). This region is called the Critical Volume V_{cr} (*Figure 2.1(a)*). Electrons are required for avalanches to begin - for positive polarity these primary electrons become available via field-induced detachment from negative ions present in the critical volume. For negative polarity, electrons are emitted from the metallic cathode via field emission. Electron avalanche ionisation takes place.

Furthermore, once the streamer inception criterion (Equation 2.1 below) is met, filamentary streamers form and protrude out of the critical volume.

$$\int_0^{x_{cr}} \overline{\alpha} \ dx > \mathrm{K} \tag{2.1}$$

where :

$\bar{\alpha}(E)$ is the field dependent net ionisation coefficient,

x is the co-ordinate on the electric field line along which the streamer develops and K is an approximate constant determined by the critical avalanche size needed for streamer propagation [12].

The first avalanches emit photoionising quanta which initiate streamers at other locations and in this manner a complex pattern of streamers is formed. These streamers propagate into the gap and form the first corona (*Figure 2.1(b)*).

The first corona has quite a well defined boundary. The streamers stop propagating at the boundary when the conditions for streamer propagation at the streamer tips are not fulfilled any longer. When this happens, the electrons in the streamer channels get rapidly attached . This leads to a number of positive and negative ions being left in the channels. There are two important physical processes that occur in the channels remaining from the first corona formation. One is that the streamer channels expand thermally because of the energy that was injected into them during the corona formation. The other is that the positive and negative ions drift apart. These two processes cause two different leader inception mechanisms, the former leads to the Stem mechanism and the latter initiates the Leader Precursor (S and P respectively in *Figure 2.1(c)*).

The Stem mechanism occurs only under negative voltages and even then not as often as Precursor formation. As can be seen in *Figure 2.1(c)*, the corona pattern is a branched tree-like structure with central stems from which branches emerge. If enough branch channels feed current into a central stem, this central channel will expand thermally due to the energy input. With expansion comes reduction of the gas density in the channel. The critical field is dependent on gas density and it, too, therefore reduces until the applied electric field is greater than this new critical field and consequently avalanche activity begins in the stem channel. The stem thus becomes a conductive path from the electrode to the corona boundary and acts as a virtual electrode (i.e. a *Leader*) from which another corona can be launched. The stem thus starts at the electrode and propagates towards the corona boundary.

More often, the mechanism that creates the Leader is the Precursor. The ions left behind in the channel drift apart due to electrostatic forces - the negative ions towards the anode and the positive ions towards the cathode. The electric field near the corona periphery is close to E_{cr}, and the incremental potential developed between the opposite polarity ions drifting apart increases the electric field by ΔE. This means the critical field is exceeded and ionisation activity begins anew. The increase in current due to ionisation activity soon leads to field distortion making the process unstable and leading to further avalanches. The filament soon becomes conductive when the current reaches the electrode and a leader is formed. The Precursor therefore starts at the corona boundary and propagates towards the electrode.

Once a leader section is formed (by either mechanism mentioned), it serves as a virtual electrode which is a conductive channel from the periphery of the primary corona to the point electrode. A second corona is launched from the leader tip further into the gap (*Figure 2.1(d)* shows secondary corona from leaders formed by both mechanisms). The second corona injects more current into the leader channel leading to increased ohmic heating and thermal expansion of the leader. Eventually the gas in the leader channel dissociates (dissociation is the breaking up of the molecules in the gas into its component atoms or into different smaller molecules. High temperatures are needed for the dissociation of the gas - about 2000 K in SF_6). As a result of dissociation, the attachment ability of SF_6 is diminished and consequently the value of the critical electric field in the dissociated region becomes smaller. The critical field in the leader is strongly reduced , a plasma channel is thus formed. The leader now has strongly reduced further heating and a low voltage drop. The potential at the leader tip is therefore close to that of the electrode.

The processes discussed are now repeated and the leader extends into the gap in jagged steps until in reaches the plane and thus bridges the gap completely and breakdown is said to have occurred (*Figure 2.1(e)*).

Chapter 3. Theoretical Simulation of Discharges

In this chapter, the methods currently available to theoretically model discharges are discussed. These methods have been comprehensively researched and a principal conclusion is that despite the availability of high-speed computers, theoretical computations of discharge processes have not progressed to the point of providing a general accurate model for the entire discharge process in SF_6. Some of these methods however show promise of success with future availability of even greater computing power. Also, the results generated by some theoretical models for specific regions of the discharge process compare favourably with experimental observations and provide useful clues towards the development of a semi-empirical model for corona stabilised breakdown which is presented in Chapters 5 and 6.

3.1 Introduction

The purpose of this chapter is to outline the various theoretical methods that may be used to simulate a discharge in a gaseous dielectric. The details of how these methods may be implemented are not covered in much depth, rather, the results that may be obtained by these methods and their ability to simulate space charge will be analysed. The merits, successes and shortcomings of the various methods are presented.

The ideal model of any physical process is given by a set, or sets, of theoretical equations; the solutions of which provide a simulation of the behaviour of the process. These equations may describe the behaviour of the microscopic elements (particles) that participate in the process or they may describe the process macroscopically. Both categories of theoretical simulation are discussed. Also, the very complex nature of breakdown in SF_6 may only be predicted by methods that can simulate non-deterministic processes. Fractal models and the stochastic nature of the discharges are therefore also discussed here.

Specifically, the following topics are discussed :

- Analytical Closed-Form Solutions.
- Boltzmann Equation Analysis.

- Continuity Equation Solution Methods.
- Monte-Carlo Methods.
- Fractals and Stochastic modelling.

3.2 Analytical Closed-Form Solutions

These methods were the first employed to attempt corona discharge modelling since they originate in a time when computer-simulations were unavailable. They are still used today since closed-form solutions have certain advantages over computer simulations. Sigmond [21] provides a detailed critical review of the methods used to solve the "space charge flow problem" and points out that computer simulations only solve parts of the problem region whereas analytical formulas cover whole regions of parameter space in a continuous way. Also, characteristic lengths and times within a corona event may easily span six decades, from microns and nanoseconds (in the ionisation region) to centimeters (or even meters in large gaps) to milliseconds across the drift region. Thus even with the aid of a powerful computer, simulating the event over the entire duration thus becomes prohibitively time consuming and costly.

These analytical methods involve deriving closed-form equations to solve for the flow of charged particles in the discharge, these complex equations are then simplified by making certain assumptions which allow a solution to be obtained. One of the most common assumptions made is referred to as the *Deutsch Approximation*, which is that the space charge ion flow in a discharge will only alter the magnitude, not the direction, of the electric field lines along which ion-flow occurs. Sigmond [21,22] and Wintle [23,24] discuss these methods of solution in depth.

The main conclusion drawn in relation to the ability of these methods to simulate corona stabilisation in SF_6 is that the nature of the approximations made will not produce accurate results. For instance, the discussion in Chapter 4 and Chapter 5 will show that the modification of the direction of the electric field lines by space charge is a key controlling factor in corona stabilised breakdown - the Deutsch approximation thus does not hold. Furthermore, the assumptions made in these analytical methods account only for unipolar space charge flow, whereas bipolar effects are significant in the discharge processes in an attaching gas such as SF_6.

3.3 Boltzmann Equation Analysis

The Boltzmann transport equation is a mathematical relation which specifies the phase-space distribution function for any given assembly of particles. This mathematical equation is known as the Boltzmann (transport) equation with the word "transport" often omitted. The Boltzmann equation allows the determination of the distribution of a particle's velocity and position in velocity and physical space. The equation is presented below, with a full derivation in Appendix A.

$$\frac{\partial f}{\partial t}+\mathrm{v}\cdot\frac{\partial f}{\partial r}+\gamma\cdot\frac{\partial f}{\partial v}=\left(\frac{\partial f}{\partial t}\right)_c \tag{3.1}$$

where : f is the function giving the velocity distribution of the particles

m.γ is the external force acting on each particle

v is the velocity-space vector

In a time interval dt the particles will be displaced by vdt and their velocities will be altered by γdt

This equation says that the distribution function of a particle in a gas changes with time due to:

- Particle motion or drift in physical space.
- Change in particle velocity due to an externally applied force.
- Collision between particles.

Although the solution of the Boltzmann equation constitutes one of the basic foundations of almost all theoretical and rigorous mathematical descriptions of plasma dynamics, its application in modelling non-uniform field discharge in SF_6 has been limited. It is apparent that solving equation 3.1 for just one charged particle species, rather than three, would require lengthy computation. Davies [25] therefore states that "even with very powerful computers...the simulation of complete discharge development using...Boltzmann techniques will not be possible in the near future." However, Boltzmann equation analysis has been applied to calculating the transport parameters, or "swarm" parameters as they are called, of electrons in SF_6 such as the drift velocity, diffusion coefficients and ionisation and attachment coefficients, e.g.

Date et al [26]. These parameters are important in other theoretical and semi-empirical models.

3.4 Continuity Equation Solution Method

3.4.1 Description

The continuity equations are essentially the equations describing the dynamics of the various charged particle species involved in the discharge. A derivation of a general equation of continuity for any particular charged particle species is given in Appendix B. The one-dimensional continuity equations for electrons, positive ions and negative ions are given by equations 3.2, 3.3 and 3.4 respectively :

$$\frac{\partial N_e}{\partial t} = S + N_e\alpha|W_e| - N_e\eta|W_e| - N_eN_p\beta - \frac{\partial(N_eW_e)}{\partial x} + \frac{\partial}{\partial x}\left(D\frac{\partial N_e}{\partial x}\right) \quad (3.2)$$

$$\frac{\partial N_p}{\partial t} = S + N_e\alpha|W_e| - N_eN_p\beta - N_nN_p\beta - \frac{\partial(N_pW_p)}{\partial x} \quad (3.3)$$

$$\frac{\partial N_n}{\partial t} = N_e\eta|W_e| - N_nN_p\beta - \frac{\partial(N_nW_n)}{\partial x} \quad (3.4)$$

where :

x = distance from anode

N_e , N_p , N_n = electron, positive ion, negative ion densities respectively

W_e , W_p , W_n =electron, positive ion, negative ion drift velocities respectively

α , η , β , D = ionisation, attachment, recombination, electron diffusion coefficients respectively (note that same value is used for ion-ion recombination as well as electron-ion recombination)

S is the source term due to photoionisation.

3.4.2 Simulation of Positive Corona in a Point-Plane Geometry

The most significant work in modelling discharge in SF_6 using this method has been done by Morrow [27,28,29,30]. The transport property data required for the solution of the above equations (i.e. the ionisation, attachment, recombination and electron diffusion coefficients) have been also compiled in a survey by Morrow [31]. Morrow solved for the discharge current in a single streamer filament of a discharge in a positive point-plane gap in SF_6 at 100kPa with a impulse voltage of a peak value of 200kV applied to the system. The evolution of the ions and electrons is described by the continuity equations above, and the space-charge electric fields accounted for by simultaneous solution of Poisson's equation (equation 3.5 below) :

$$\nabla \cdot \left[J + \varepsilon_0 \frac{\partial E}{\partial t} \right] = 0 \tag{3.5}$$

where : the current density $J = e(N_p W_p - N_n W_n - N_e W_e)$.

State of the art numerical techniques were developed by Morrow and Cram [32] to solve this complex system of equations. Although a powerful Cray computer was used for the simulation, the streamer was only simulated over a time span of about 30 nanoseconds [27].

3.4.3 Results of Morrow's Simulation

The important results of the simulation were:

- Streamers form very quickly - the streamer forms at a velocity an order of magnitude greater than the electron drift velocity (at the critical electric field).
- As the applied voltage rises, the initial rapid streamer formation causes corona onset pulses in the current. These sub-nanosecond current pulses agree with experiment [28].
- The electric field in the trail of the streamer is approximately equal to the critical electric field.
- The distribution of space charge in the streamer channel, i.e. positive ions at the streamer tip and electrons closer to the anode, also accounts for the pulses of current which are caused by further avalanche activity.

Morrow's results were important in the development of the semi-empirical model by Wiegart et al [5] which is the most accurate model to date of inhomogeneous field breakdown in SF_6 under fast impulses.

A criticism of Morrow's method is that it may be accurate for the simulation of discharges in uniform fields but the results in nonuniform fields may not be accurate for the following reason : In the uniform field case, the electron swarm parameters; namely the ionisation coefficients, attachment coefficienta, drift velocity and diffusion coefficients are treated as independent of space and time. They are a function of electric field only, or rather a function of local E/N (E is the electric field strength and N the gas number density). The assumption is that the electrons have reached a state of hydrodynamic equilibrium with the field. In highly nonuniform fields, this equilibrium is not attained since the field is changing quickly and the energy gained by the electrons from the field cannot be balanced by energy loss by collisions. The swarm parameter values are thus not the same as those predicted using local field values. Morrow's simulations do not account for swarm parameter variation.

3.5 Monte-Carlo Methods

Together with the continuity equation methods discussed in 3.4 above, the most successful non-empirical simulations of discharge processes in SF_6 have been achieved by the Monte Carlo method. The state of the art in Monte Carlo simulation of discharges in SF_6 is found in the work of Liu and Raju [33,34,35]. A flow chart of the Monte Carlo method of simulation used by Liu and Raju is reproduced in *Figure 3.1*.

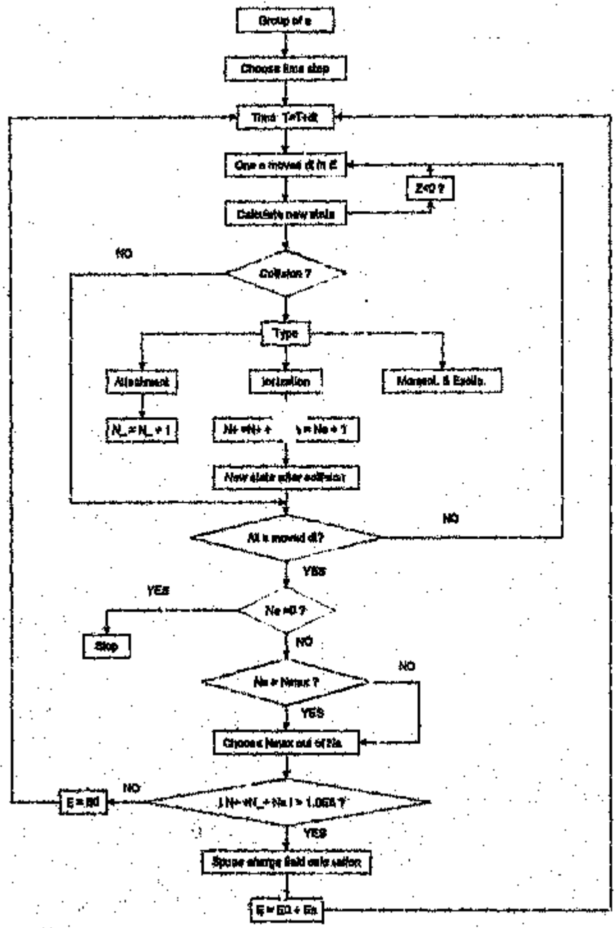

Figure 3.1 Flowchart of Monte Carlo simulation of discharge [34]. e = electron, Ne = number of electrons, N+ = number of positive ions, N- = number of negative ions.

The significant results of these simulations are :

- As in Morrow's simulations (cf. Section 3.4) in the Monte Carlo simulations, corona currents under positive overvoltages in a needle-plane geometry were found to occur as a *burst of pulses*. The occurrence of these pulses need to be accounted for in any description of the physical processes that take place in a discharge - the qualitative model of corona stabilisation presented in Chapter 5 does account for the pulse characteristic of the current.

- The simulations show that the development of avalanches and streamers are due to ionisation and photoionisation, whereas the quenching of the avalanches and streamers are due to space charge fields.
- It is also shown that in positive corona the electric field is depressed near the tip of the anode and enhanced in the rest of the region. This result further confirms the mechanism by which positive-ion space charge acts in the corona stabilised breakdown. This is discussed in Chapter 5.
- Another result of the simulation of positive corona is that the concentration of negative ions is smaller than that for the positive ions.

The Monte Carlo method is thought to produce a more accurate solution than the continuity equation solution method. This is because the Monte Carlo method essentially simulates the motion of individual particles participating in the discharge and uses probabilistic methods to determine the collision behaviour of the particles - there is thus no need to use approximate swarm parameters as is the case with continuity equation solutions (cf. Section 3.4.3). However, it suffers from the same shortcoming as other numerical methods of discharge simulation - it cannot model the breakdown event over its entire duration.

3.6 Fractal Models and Chaos Theory

The theory of fractals may be considered to be a subset of the more general Chaos theory, but they will be considered separately here.

Chaos theory is essentially a science primarily concerned with a system's sensitive dependence on initial conditions - that is, certain physical systems seem very deterministic until some small change in initial conditions leads to complicated, seemingly random motions. A good introduction to the field has been written by Peitgen et al [36]. This theory has been successfully applied to modelling certain complicated physical processes such as fluid-flow. Van Brunt [2] states that partial discharge does exhibit "chaotic, nonstationary, or fractal type behaviour". It therefore was necessary to investigate the possibility of using this theory to model discharge.

3.6.1 Chaos Theory in Modelling Discharges

Chaos theory is currently inapplicable to the modelling of concern in this thesis. Chaos theory is essentially used as a tool for *confidence determination.* That is, in a system that exhibits chaotic behaviour and if that system's behaviour is well understood under certain conditions, chaos theory is used to determine the range of conditions in which predictions made do apply and the confidence level of those predictions. The salient point is that the system is quite well understood and that there usually also exists quite a vast amount of empirical data on the system under "normal" conditions as well as "chaotic" conditions. In the case of the problem at hand, i.e. *quantitatively describing the effect of charges deposited by previous corona events on subsequent discharges* , there is very little known about the phenomena involved (especially at the microscopic level), and furthermore there is little or no empirical data describing the phenomenon. In other words there is no quantitative model describing the phenomenon of corona stabilisation, and therefore chaos theory (which will determine the effect of changing initial conditions on the outcome of the events) cannot yet be applied. It is true that fluid flow is similar in many respects to partial discharge events in that, for instance, they both are described by simultaneous non-linear partial differential equations. However, chaos theory is being applied to fluid flow models quite successfully and it has not yet been applied to gas discharge. The reason for this is that there is very much more empirical data on fluid flow and consequently there are models for the fluid flow phenomena to which chaos theory can be applied. There is much less data on corona stabilisation phenomena and no models currently exist.

3.6.2 Discharge Modelling using Fractals

About two decades ago, Mandelbrot [37] developed the theory of fractals. Fractals are used to model mathematically and accurately describe phenomena and shapes that occur in nature. These shapes are often characterised by a high degree of complexity and irregularity. A detailed description of what fractals are cannot be made here. Peitgen et al [36] serves as a good introduction to fractal theory.

Unlike Chaos theory, fractals have been used in the modelling of discharges in solids, liquids and gases with limited success. A single published work [38] describes the application of fractals to discharges specifically in SF_6 where it is merely shown that simple stochastic models naturally lead to fractal structures for the pattern of the discharge. Other works in the use of fractals to model discharges are by Pietronero et al [39,40], Barclay et al [41] and Egiziano et al [42]. The conclusions reached from a study of these works are :

- Fractal models currently do not represent complete theoretical descriptions of the discharge process.
- Fractal models merely reproduce the filamentary tree-like structures of discharge patterns. They do not contain any information about the time development of the discharge.
- It is difficult to make meaningful quantitative comparisons between the fractal model and experimental observations.
- Current fractal models do not account, or make simplifying assumptions, for microscopic mechanisms in the discharge.

For these reasons it is clear that fractal models cannot be usefully employed to model corona stabilised breakdown.

3.7 Stochastic Modelling

Stochastic processes are generally viewed as the "dynamic" part of probability theory. One is observing a stochastic process when one examines a process developing in time in a manner controlled by probabilistic laws. Partial discharge phenomena are considered to be stochastic because their properties are describable in terms of a set of time-dependent random variables. The stochastic nature of SF_6 discharges has been studied in depth by Van Brunt [9], this work being mainly experimental and thus will be discussed in Chapter 4. Van Brunt [9] states that "a theoretical (stochastic) model of positive-corona pulse bursts ... does not yet exist". There are no models that quantify the stochastic nature of discharges in SF_6.

3.8 Conclusion

It is apparent from the foregoing discussions that purely theoretical methods of discharge simulation are inadequate for modelling ion-drift controlled corona stabilised discharge. The salient reasons for this are :

- Most methods are only capable of performing the simulation at a fixed overvoltage, whereas it is clear that the rate of change of applied voltage is a key factor in corona stabilisation. Those methods that do have a changing voltage as an input to the simulation (such as Morrow's method of solution of the continuity equations) are not yet able to model the process for a long enough period of time, primarily due to the limitations of computing power. Also, the aforementioned method only models a single streamer channel, and it is the simulation of the interaction between many such channels in a corona cloud that is required for a complete model.
- The requirements of computational time are significant in most numerically implemented models, especially for the microscopic models such as the Monte Carlo and Boltzmann equations. There are no simulations to date that have modelled the entire discharge process in inhomogeneous fields in attaching gases such as SF_6.

Chapter 4. Analysis of Previous Work on Corona Stabilisation

The conclusion reached in the previous chapter, which studied theoretical methods of modelling discharges, is that there are no numerical models currently able to simulate corona stabilised breakdown. In this chapter, previous attempts at modelling corona stabilised breakdown are examined and empirical work done by researchers pertinent to this type of SF_6 discharge is studied. This information is used to present a qualitative description of the mechanism of corona stabilised breakdown in Chapter 5 which leads to a quantitative model which is presented in Chapter 6.

4.1 Introduction

In studying the previous work done in the study of the corona stabilisation mechanism in SF_6, it has been established that only the broad description of the phenomenon is agreed upon by all researchers. That is, corona stabilised breakdown occurs in highly nonlinear fields in SF_6 when positive voltage waveforms of slow rise-times are applied. Also, there is agreement on the fact that this phenomenon occurs within a certain pressure zone, and that the operating pressure of most SF_6 insulated equipment falls within this pressure zone which lies between approximately 100 and 400 kPa. At pressures below about 100 kPa, breakdown occurs purely via the streamer mechanism - that is, there is no leader formation and breakdown occurs when a streamer crosses the gap. At high pressures, "direct breakdown" is said to occur. In this case, the voltage at which breakdown takes place is equal to the streamer formation voltage. The prediction of the zone of pressure in which corona stabilisation occurs is dealt with by Pinnekamp et al [18,19,20] and Wiegart et al [5].

4.2 Leader Launch Angle Analysis of Corona Stabilisation

This section discusses the significant work of Van Der Zel [8,11] who devised some unique experimental techniques the results of which provide clarifying information on the nature of corona stabilised breakdown.

In order to verify the various postulates stated about breakdown under corona stabilisation, the phenomenon was experimentally investigated using a unique measurement method which involved measuring the launch angle of the leader stroke that emerges from the streamer while simultaneously measuring the time to breakdown. The results showed that under switching impulses, there was indeed a correlation between leader launch angle [illegible] to breakdown. The launch angles for an 84 microsecond rise-time switching impulse were shown to be spread in two distinct distributions, some angles were distributed below 60 degrees and others above that angle. Furthermore, the time to breakdown for the sparks that occurred at angles below 60 degrees were all below an average of 100 microseconds with a small spread in the values whereas the sparks that launched at angles greater than 60 degrees took 200 to 300 microseconds to cross the gap and the spread of breakdown times at each angle was very large (standard deviations as high as 388 microseconds were measured).

Van Der Zel adopts the postulate of Niemeyer et al [17] that the corona is a compact structure with a well defined spherical envelope. He uses a model of the corona being an equivalent conducting sphere of radius roughly equal to the diameter of the rod-tip (*Figure 4.1*) and postulates that breakdown in the presence of corona stabilisation will produce spark paths with launch angles distributed about launch angles between 45 and 90 degrees.

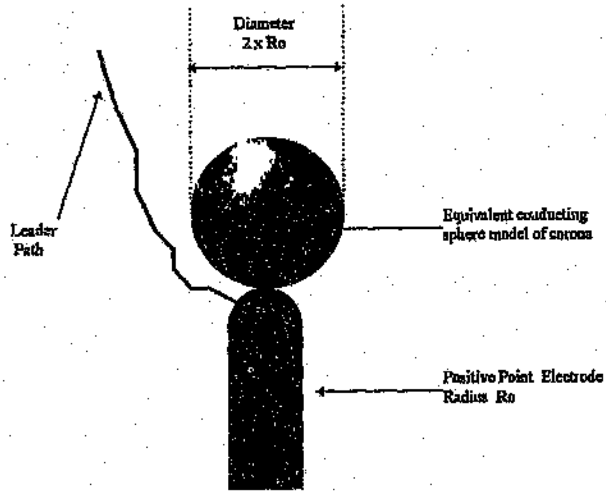

Figure 4.1 Leader Path in Corona Stabilised Breakdown

A significant finding was that breakdown both with and without corona stabilisation occurs for switching impulses. Breakdown without corona stabilisation under switching impulses is not expected since the statistical time lag for a small diameter rod (1mm) is about 1 microsecond [8]. This means that approximately one microsecond after the critical voltage is exceeded, corona stabilisation should form, and since the rise-time of the switching impulse is in the order of tens of microseconds, one would expect corona stabilisation to occur for every switching impulse. The explanation for this behaviour lies in the "sweep field" effect : The slow rising voltage allows negative ions to drift out of the critical volume and therefore there are no electrons available between $V_{applied}=V_{critical}$ and $V_{applied}=V_{leader}$, so the electron becomes available only when $V_{applied}>V_{leaderonset}$ (by this time the positive ions will have drifted away from point thus nullifying their electric field reducing effect). Hence the very first streamer that is formed meets the leader inception criteria, and thus direct breakdown takes place.

4.3 Attempts at Modelling Corona Stabilised Breakdown

An early attempt to model breakdown in the corona stabilisation zone was by Chatterton [43]. The flaw in this model, and indeed most other attempts at modelling the phenomenon, is that the *only mechanism for breakdown considered is the streamer theory*. In this model, the initial corona inception is estimated using the streamer-inception criterion and the radius of the initial corona cloud estimated to be that of the critical volume. This streamer corona is taken to be growing as the voltage is increased until a limiting radius is reached where photoabsorption prevents further multiple streamer formation. The electrode radius is replaced with the effective corona cloud radius (*Figure 4.2* below). Also, it is assumed that there is no voltage drop across the cloud and the potential at this radius is taken to be that of the electrode. The voltage predicted by the Nitta-Shibuya [44] streamer inception voltage equation (and replacing the rod radius with the largest corona cloud radius) is taken to be the breakdown voltage.

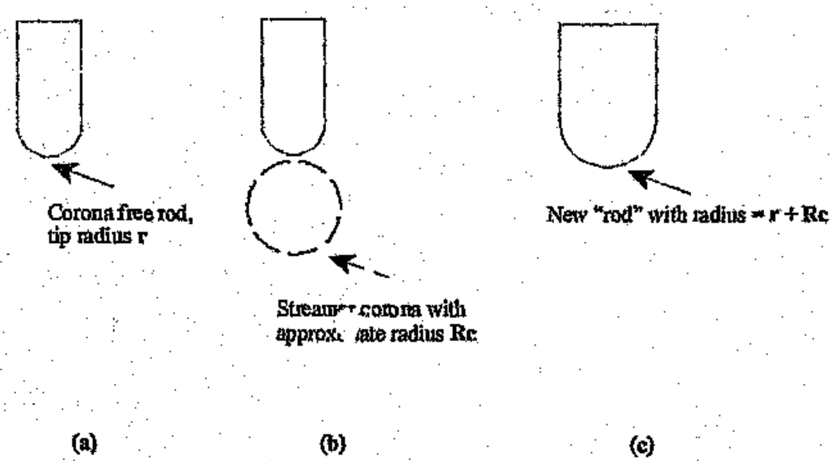

Figure 4.2 The "Virtual Rod" Concept

The model results were compared to two sets of measurements (using two geometries) with impulse voltages. The results of their model were more accurate at low pressures (where the streamer mechanism does dominate). At pressures below the critical pressure, they had to allow some physical constants to vary in order to obtain some degree of agreement between the model and measurements. The model was even more inaccurate at pressures above the critical pressure - this is because the leader precursor mechanism dominates here. There is also a contention that the "space charges reduce the field around the point and *have to be extensive enough to prevent alternative breakdown paths around the edge of the corona cloud.*" - this has been disproved by Van der Zel [8].

Nelson [45] shows that the simple corona cloud model does not apply at higher pressures (>1atm) and divergent field conditions (0,5mm point). Optical multichannel analysis was used to measure the corona size under various conditions of pressure and tip geometry. Nelson found that at low pressure (50 kPa) there was no limit to the size of the corona cloud, whereas at higher pressures, the corona cloud radius reached a limiting size and had a well defined envelope. The model Nelson presents in his work merely attempts to predict the radius of the corona cloud at higher pressures. The model results, when compared to experimental optical measurement of the corona radius, predicts smaller corona radii. The author ascribes the discrepancy to the possibility of streamers growing out of the corona cloud which are not accounted for in the model as well as the fact that he regards the model as a crude approximation of the physics. The work of Wiegart et al [5] was more successful at predicting the radius of the streamer corona envelope under positive impulses and will therefore be used in the model in Chapter 6.

Also an early attempt to quantify breakdown under corona stabilisation was made by Abdel-Salam et al [46] where a semi-empirical corona-cloud model is also used to calculate breakdown voltage. The criterion is expressed in the following equation :

$$\int_0^{x_e}(\alpha-\eta)dx = Z\frac{x_e}{a} \qquad (1)$$

The value of Z is found for a given geometry by calculating the left hand side of the equation at the experimental breakdown voltage. The values of α and η (the ionization and attachment coefficients respectively) are evaluated with the space charge field of positive ions accounted for. From calculation of the electric field in the gap and the values of α and η the avalanche length x_e is determined. Z is obtained from the above equation (given that a is the radius of the electrode). Once Z is known, both sides of the equation are calculated at different voltages above the corona onset value. The voltage that satisfies the equation is then considered to be the breakdown voltage.

Parekh and Srivastava [47,48] show that the method proposed above does not work. They further go on to show that "there seems to be no simple equation that can correlate discharge parameters, the field non-uniformity, the gas pressure and breakdown voltage" for positive impulse breakdown in non-uniform geometries.

Clearly, the only breakdown mechanism known to researchers at that time - the streamer mechanism, was inept at predicting breakdown at pressures higher than about 100 kPa and in very non-uniform geometries. All model attempts made were based on some form of streamer criterion. There has been no published attempt to quantitatively include corona stabilisation in any modern model that is based upon the leader precursor theory.

4.4 Other Significant Experimental Investigations

4.4.1 Pulse Characteristics of SF_6 Discharges

The work of Anis et al [49] provides useful data on the breakdown behaviour of SF_6 in a point-plane arrangement under applied positive switching impulse voltages. Rod diameters from 1 to 10mm were used in a 50mm gap and under impulse front durations of 30, 170 and 350 microseconds. Based on discharge-current measurements, they subdivided the discharge behaviour into four categories - "direct breakdown", "incomplete breakdown", "single-pulse discharge" and "multiple-pulse discharge".

At high pressures, direct breakdown was predominant which is referred to by the authors as corona-free breakdown since the only discharge event measured was the breakdown itself. Again, in the absence of the leader mechanism theory of breakdown, the authors attribute direct breakdown to a streamer crossing the gap.

The authors refer to the occurrence of a single discharge pulse well within the prospective time-to-breakdown without breakdown ever taking place as incomplete breakdown. It should be noted that the size of the discharge events (measured as current pulses) in the case of incomplete breakdowns were 30 to 100% larger in magnitude than single discharge pulses.

In single-pulse discharge, a single current pulse clearly precedes the breakdown event. It was found that there could be a delay of up to a few hundred microseconds under an applied pulse of 350 microsecond front duration. It was found that these long delays between initial discharge and breakdown always occurred in a particular pressure zone and especially with small diameter needles. This pressure zone is referred to the authors as the corona-stabilization pressure zone. The pressure above which direct breakdown predominates is termed the critical pressure. The pressure zone below this critical value is where the probability of occurrence of single pulse discharge is greatest. Of significance is the observation that this form of single pulse discharge occurs most frequently for the most nonlinear geometry and occurs seldomly in the case of the 6mm diameter rod. This is because corona inception voltage is reached later in the case of the 6mm rod than for a smaller diameter rod (which has more nonlinear field), and the inception voltage will be very close to the breakdown- or leader formation- voltage for the thicker rod therefore direct breakdown is more likely for the 6mm rod case.

The data obtained from this work provides a measure of confidence in modelling corona stabilisation by *only considering the initial streamer corona* (which accounts for the large single current pulse).

4.4.2 Effect of Injected Space Charges on Positive Impulse Breakdown

Qiu et al [50] injected positive and negative polarity charges into a point-plane gap by auxiliary needle electrodes surrounding the gap. A 1,5/50 microsecond impulse was applied to the point plane gap. It was found that injecting negative charges decreased the impulse breakdown voltage significantly but had no effect on the impulse strength before the inception voltage was reached. The conclusion drawn from this was that the injected charge had no effect on initial streamer formation but provided seed electrons in the gap for the subsequent leader steps.

It was postulated that the injected positive ions would have little effect on the initial streamer-leader formation since in a fast lightning impulse, the ions would not have enough time to modify the field around the needle tip. This was verified. Furthermore, the concept of a "sweep-field" which sweeps the negative ions out of the critical region thus depriving the corona of a seed electron may contribute to some higher breakdown values in the case of a fast impulse (confirmed by Van Der Zel [8]) .

4.4.3 Gas Mixtures

The experiments investigating the breakdown behaviour of SF_6 doped with other gases assists in understanding corona stabilisation in pure SF_6.

Nelson [51] doped SF_6 by small quantities of triethylamine and found that this increases corona activity in the critical volume. This is because triethylamine has a low ionization potential of about 7,5eV which corresponds to a spectral energy at which SF_6 has a much lower photoabsorption coefficient (approximately $0{,}1cm^{-1}$). With increased corona activity it was observed that corona stabilisation was more pronounced. This indicates the influence of the magnitude of the initial corona on the probability of corona stabilisation occurring. The implication of this postulate for modelling is that the primary corona should be modelled because of its significant influence.

Mufti et al [52] performed experimental investigations on the behaviour of corona discharges from free conducting wire particles in SF_6 and its mixtures which confirms Nelson's work [51] that adding triethylamine enhances corona stabilisation. The significance of this paper to the model presented in Chapter 6 is that it indicates that the same physical effects that apply for a fixed particle may be applied to free particles (with additions and modifications).

In their work on SF_6-Freon mixtures, Farish et al [53] found that larger impulse coronas tend to suppress leader formation because of their space-charge shielding effect. They also postulate that since the impulse corona comprises a large number of individual streamer filaments, the enhanced shielding effect of an increased number of streamers may be more important than any increase in the charge per filament. The probability of leader development at a given voltage would then depend on the statistics of initiation of an effective shielding corona. They found that the competing effects of an increase in the number of streamer channels formed (which enhances corona stabilisation) and an increase in the charge density per channel (which promotes leader formation) make interpretation of charge measured in impulse coronas difficult. The charge deployed in the discharge is thus a critical factor in determining a quantitative prediction of corona stabilised breakdown - this is addressed in Chapter 6 and the problem of measuring the true charge deployed in a discharge is discussed in Chapter 7.

4.5 Stochastic Nature of SF_6 Discharges

The most significant work done in studying discharges in SF_6 from the perspective that the nature of the discharge is stochastic, is by Van Brunt [54]. He found that positive corona in electronegative gases exhibits a pulse burst characteristic in highly non-uniform fields - i.e. discharges appear as a series of randomly spaced groups of pulses where the spacing between pulses is much smaller than the spacing between successive groups. He also states that a theoretical model of positive corona pulse bursts from which quantitative predictions can be made does not yet exist. Despite this lack of any rigorous treatments of the pulse burst characteristic, in this thesis, a postulate for the mechanism causing the pulse nature is given in Chapter 5.

4.6 Conclusion

Clearly, all the empirical studies of relevance to corona stabilisation are too numerous to discuss here. In this chapter, the work considered to be most beneficial to developing a hypothesis of the mechanism of corona stabilised breakdown (and from this a quantitative model) was expounded. The discussions presented here provide justification for many of the assumptions made in the following chapter in which an attempt is made to present a theory that fits all the empirical characteristics of corona stabilised discharge.

Chapter 5. Qualitative Model of Breakdown under Corona Stabilisation

Chapter 3 and Chapter 4 presented analyses of theoretical modelling and empirical investigations of discharge and breakdown in SF_6. Based on the information analysed previously, a qualitative theory of how corona stabilisation occurs is propounded in this chapter. There is no commonly accepted rigorous or detailed theory of how corona stabilised breakdown occurs, creating a necessity for some kind of description of the physical processes that occur around which a first quantitative model may be constructed. These processes are described here and the resulting quantitative model is presented in Chapter 6.

5.1 General Mechanism

In the previous chapter, earlier investigations into the corona stabilisation phenomenon were discussed. Most researchers were in concurrence as to certain mechanisms responsible for corona stabilised breakdown. Based on the study of these works, a general mechanism of corona stabilised breakdown is outlined here and illustrated in *Figure 5.1*.

Figure 5.1 shows schematically the difference between breakdowns from a point electrode to which fast rising and slowly rising positive voltages are applied. In both cases, V_c is the potential at which measurable corona (i.e. streamer corona as described in chapter 2) is formed at time t_d. In the case of the waveform with the high dV/dt, the voltage at which there is a sufficiently high field to allow leader development (V_{L1}) is reached in a short time t_{L1}. The leader almost always follows a path along the central axis of the point - i.e. the leader follows a straight path. Breakdown then occurs when the final leader step arrives at the cathode.

In the case of a slowly rising waveform, once the streamer corona is formed, there is a time lag that is long enough to allow the negative ions that remain in the streamer channels to drift back into the point anode. The only charged particle species remaining in the gap are positive ions which are drifting towards the cathode. It is believed that the presence of the positive ions decreases the field strength at the point sufficiently to prevent leader formation even though the applied voltage is at a high enough level that would cause leader inception in the absence of the positive charge. The positive ion distribution thus acts antagonistically to the applied voltage. As time elapses, the applied voltage increases further and the ions drift farther away from the point. A stage is thus reached when the applied voltage overcomes the opposing effect of the positive ions and a leader is allowed to form. The leader path is curved, indicating that the ions have not drifted far enough away so that they do not have an influence of the field.

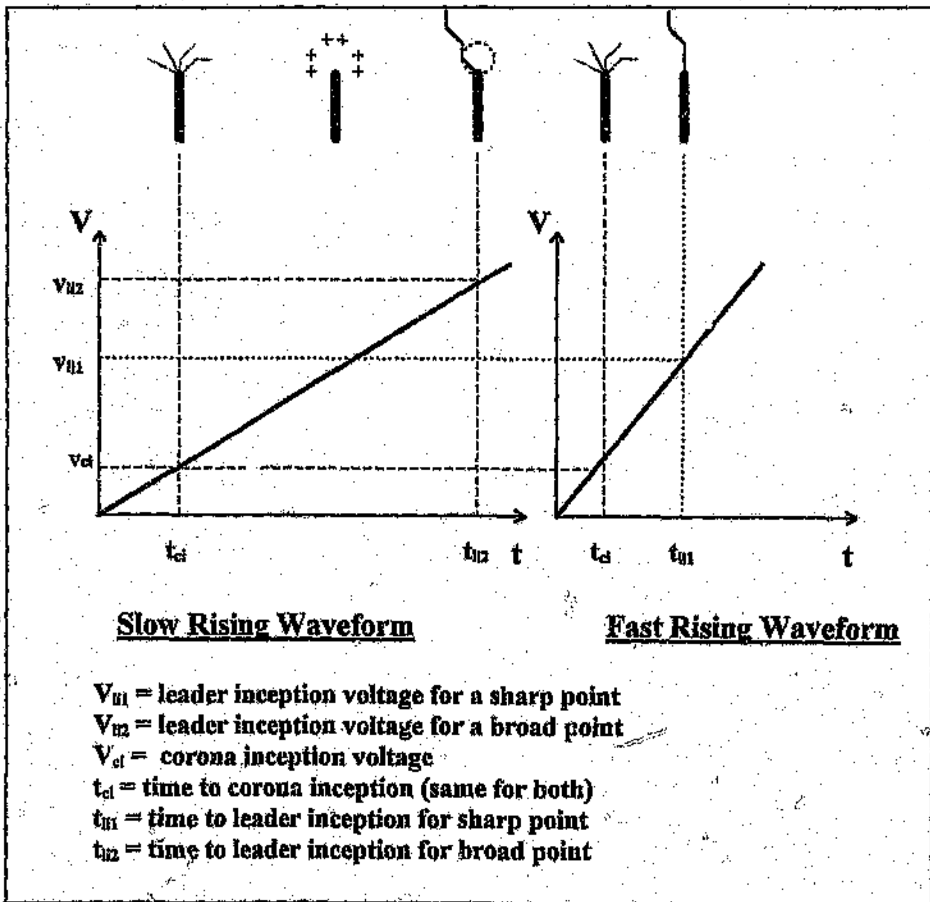

Figure 5.1 Breakdown from a point electrode under slow and fast rising positive waveforms

5.2 Finite Elements Model

The characteristics of the corona ion sheath or "cloud" and its influence on the electric field distribution was evaluated using a finite elements model.

The finite elements model was used to test the "equivalent rod-radius" concept of corona stabilisation which uses a conducting sphere to model the si. 'ation. A commercial finite elements package, in particular a two-dimensional axi-symmetric electrostatic solver was used. The geometries modelled were the following, corresponding to the experimental setup used by Van Der Zel [8] :

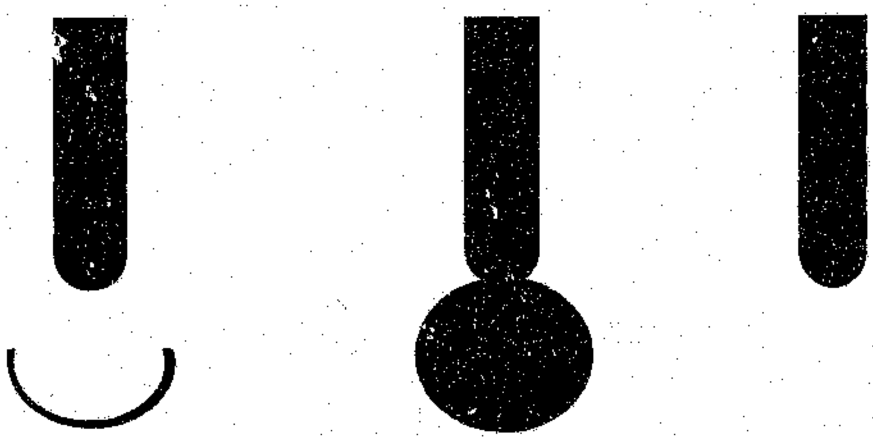

(a) (b) (c)

Figure 5.2: Models Used (Figures not to scale)

Figure 5.2(a) shows a thin (about 10μm) hemispherical shell in space around which charges are distributed , *Figure 5.2(b)* a conducting sphere at the point electrode, and *Figure 5.2(c)* shows a space-charge free point. All the points were 0,5mm in radius and the plane 20mm away. The radius of the sphere in *Figure 5.2(b)* and the radius of the arc in *Figure 5.2(a)* is 1mm. The radius of the corona sphere/hemisphere used here was determined experimentally in [8] and theoretically in [55].A voltage of 100V was applied to the rod. The actual magnitude of voltage applied is not important since we are interested in comparing the results obtained for the three geometries, and the results will thus be normalised to the maximum value.

5.2.1 Results of Finite Elements Model and Discussion

A plot of the electric field magnitude versus angle along an arc close to the tip of the rod is shown in *Figure 5.3*, the central axis of the rod corresponds to 0 degrees and the arc spans 90 degrees in an anticlockwise direction. The results for the conducting sphere are not plotted, but will be described.

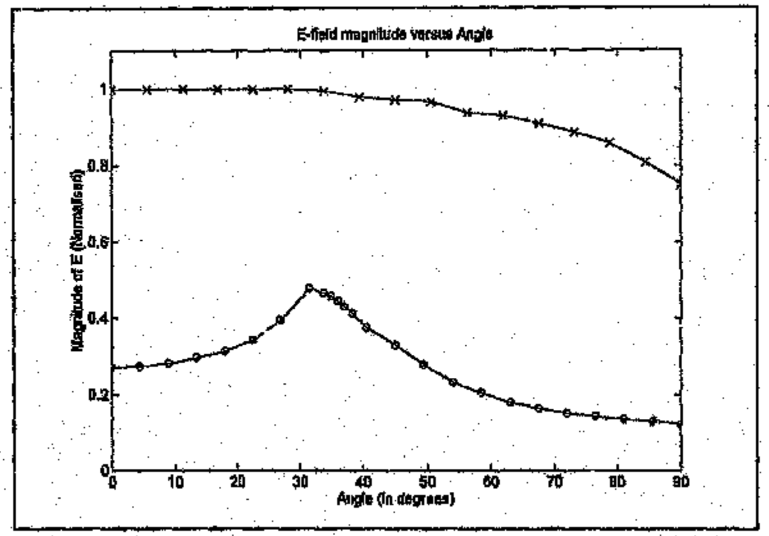

(a) x = without space charge

(b) o = hemispherical shell distribution of space charge(Q=1pC)

Figure 5.3 : E-Field magnitude versus angle along an arc in front of the tip (normalised to the maximum value)

Modelling the space charge as a conducting sphere does not seem to be the best way to do so. The field strength in the region between the sphere and the rod is highly reduced - since the sphere is conducting, it is at the same potential as the rod, so the junction forms an equipotential surface. Thus in this case, the leader will not develop at an angle, since the maximum field is found to be at the tip of the sphere - i.e. along the central axis of the point (as expected).

It is clear from the plot in *Figure 5.3* (for the space charge free point) that the maximum stress occurs when the angle is zero - that is along the central axis. By placing positive charges in a hemispherical shell distribution with a radius the same as that of the conducting sphere the results allow tentative conclusions to be drawn about leader launch angles. It is clear from the graph in *Figur . 5.3 (5.3(b)* - with space charge), that the electric field magnitude is greater along paths that are at angles greater than 0 degrees - i.e. away from the central axis. Also, as the magnitude of charge was increased, the magnitude of the field dropped accordingly. Thus the larger the amount of charge injected by the discharge, the greater the degree of stabilisation. Also, the spread of angles of leader launches found experimentally by Van Der Zel [8] (i.e. most of the leaders leaving at angles greater than about 40 degrees) have been to an extent verified - the field strength reaches a maximum at about that angle and then drops off slowly - a leader will form more easily in a higher field region.

The charged conducting sphere method is clearly not a useful device for looking at corona stabilisation effects. This model was proposed by Wiegart et al [5], because it could model corona structure effectively when calculating the critical charge necessary for leader inception - it was not meant to model the ion cloud. The idea of conceptually using a thicker "virtual point" of radius equal to the space-charge "cloud" to model stabilised breakdown will probably predict the higher breakdown voltage (since it accounts for a reduced field). It does not however describe the physical processes and will not predict the angular leader launch.

It is clear from the previous simulations that the distribution and magnitude of residual charge at the end of a discharge is the key factor controlling the field stress around the point electrode which controls the next discharge/leader formation. It is therefore important to understand how the first discharge develops in the virgin gap. From experimental evidence it has been shown that under d.c. and a.c. conditions (in a positive point-plane arrangement), discharges consist of a number of randomly spaced pulses with an initial large pulse and a trail of smaller pulses before breakdown occurs [55,56]. Any attempted physical description must be able to explain these effects.

5.3 Qualitative Description Of Physical Processes

Experimental findings show that partial discharges from point electrodes (i.e. very non-uniform fields) under positive applied stresses consist of a sequence or burst of pulses with an initial pulse of large amplitude followed by much smaller pulses [55,56].

- The first large magnitude pulse probably corresponds to the initial streamer corona as described in Chapter 2. The initial streamer propagates a considerable distance into the virgin gap. The corona structure has a roughly spherical envelope with a well defined boundary [17]. The corona consists of a complex pattern of streamer filaments which have a mainly radial spatial extension.

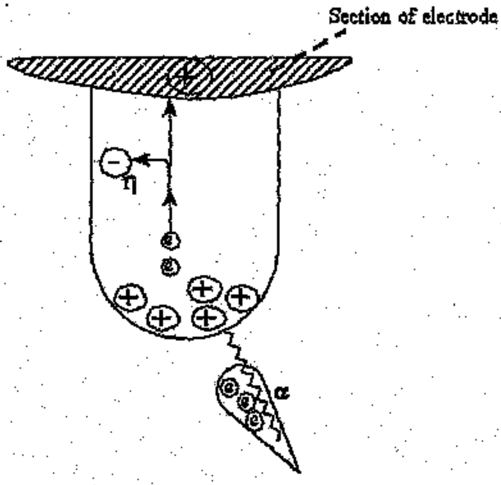

Figure 5.4 : Exaggerated view of processes that occur inside a single streamer filament

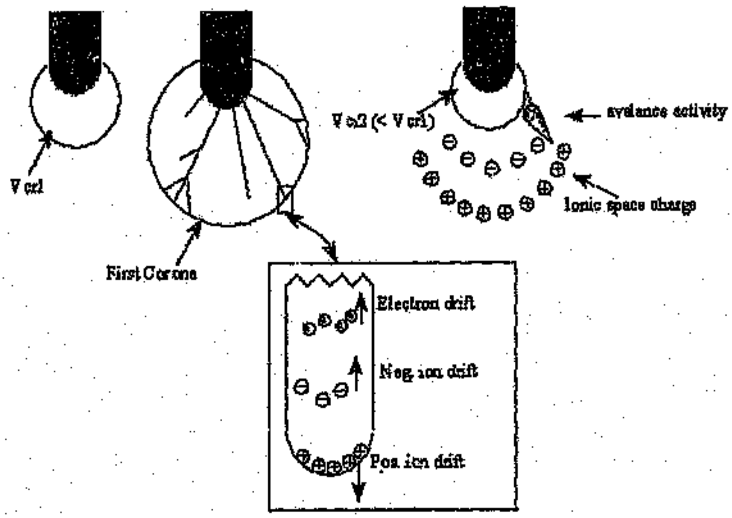

Figure 5.5 Streamer corona in SF_6

- At the tips of each streamer filament, when the corona stops growing, electrons get rapidly attached thus forming negative ions. If, at this stage the applied voltage is not high enough to cause leader precursor development (as described in Chapter 2), the highly mobile electrons in the streamer trails drift back into the anode. *Figure 5.4* is an exaggerated view of the processes that occur in at streamer filament. The discussion below may be more lucid if reference is made to *Figure 5.5*.
- The negative ions in the streamer also begin to drift back towards the anode, whereas the positive ions in the streamer tips drift towards the cathode. Since the corona boundary is roughly spherical, the positive ion distribution is assumed to be roughly hemispherical in the finite elements model described earlier .
- The positive ion distribution acts to lower the electric field magnitude around the point. However, the negative ions that are still in the region between the positive ions and the point act to increase the field at the point. Conceptually, this may be thought of as a new critical volume which is smaller in size than that in a space charge free gap. Besides causing the field enhancement, these negative ions also serve the purpose of supplying seed electrons for new avalanches. The negative

ions produce electrons via detachment and these electrons cause avalanches - these avalanches are therefore the secondary events in the measured burst of pulses. Also, the temporal distribution of the secondary pulses are found to be random, and this randomness can be explained by the probabilistic nature of field detachment from the negative ions.

- These secondary avalanches or streamers which develop in the wake of the first streamer will not propagate as far into the gap due to the shielding effect of the residual positive ion space-charge, and thus will be of lower magnitude than the primary pulse. The secondary streamers clearly leave behind more positive ions, the negative ions that are also formed have a short distance to travel to be absorbed into the anode. The number of negative ions in the gap diminish with time after the initial streamer, thus steadily reducing the probability for initiating electron formation time [55].
- In the case of a d.c. applied voltage, once a critical amount of positive charge builds up, thereby ensuring that the field in front of the anode is sub-critical everywhere, all ionisation activity stops and the measured burst of pulses also stops. After a time has elapsed that is sufficient for the positive ions to have drifted far enough away from the anode to allow a critical field to exist again, ionisation activity will restart once a first electron becomes available in this critical volume. Another pulse burst will then be measured.
- For the d.c. case, the Laplacian background field stays constant and there are thus only two factors controlling the change in the field distribution around the point - that is, the positive and negative ion distributions. For the case of a slowly rising applied impulse, the Laplacian field is also increasing slowly. The initial discharge stages will be almost the same as in the d.c. case. However, once the initial corona burst occurs, the rising voltage ensures that there is always a finite increasing critical volume surrounding the point electrode. Therefore, once the initial large corona has formed, and the positive ions form the hemispherical sheath at the corona boundary, the negative ions drifting to the anode provide the seed electrons which lead to the formation of a new streamer corona. This secondary corona will be larger than in the d.c. case because the increasing applied voltage will ensure a larger critical volume. It is clear from the Finite Elements modelling done earlier

that if a secondary streamer "brush" develops between the anode and the positive ion sheath, those filaments of the streamer that develop at angles greater than 0 degrees from the central rod axis are subjected to a larger background field. These filaments are therefore likely candidates for leader precursor formation. This explains the predominantly curved nature of leader paths. The applied voltage will have to increase to a large enough magnitude to allow the secondary streamer to produce a precursor. This explains the larger breakdown voltages under the slow impulses.

- The rate of formation of the positive ion cloud from the primary event is a key factor controlling the following discharge events. The rate of ion accumulation is dependent on the drift velocity (and thus the mobility) of positive ions in SF_6. Positive ion mobility is dependent on pressure according to an approximate inverse relationship, that is : $\mu_+ \propto \frac{1}{p}$, where μ_+ is the positive ion mobility and the pressure is given by p [5]. Therefore, at higher pressures the mobility of the ions is reduced and a faster build-up of ions could be expected to occur and therefore a corresponding increase in stabilisation.

5.4 Implications for Quantitative Modelling

We are interested in a model for breakdown under slowly rising voltages - that is, a.c. as well as slow switching impulses. Clearly, in the case of the a.c. waveform, there are discharge events that occur during the negative half cycle. The memory effects of these events may affect discharges on the next positive half cycle. There has not been any work done to date that quantifies these effects, so we will treat the a.c. case as just a slowly rising positive waveform. Furthermore, the formation of the "brush" type streamer pattern has been questioned by Farish [57], who has found that under d.c. corona, there is only one streamer filament, which is measured as the initial pulse, and the subsequent measured pulse burst is due to the re-striking of the same filament and Farish states that this is the mechanism more likely to occur for slowly rising a.c. waveforms. It has been suggested by Niemeyer [56] that the restrike mechanism operates at low voltages, and that the size and complexity of the streamer corona increases with voltage. Also it has been found that at high pressures, the bursts are very narrow and often only the single pulse appears [55]. It is therefore deemed acceptable to base a model on the concept of a single initial "brush" streamer corona. Thus a possible quantitative model accurate to a first order approximation will include the following physical effects :

- An estimate of the size of the initial streamer corona envelope. The positive-ion distribution could then be taken to be along the surface of this envelope.
- An estimate of the magnitude by which the positive-ion distribution modifies the Laplacian electric field. For a first-order model, the antagonistic effects of the negative ion distribution may be neglected, since it has been found that the concentration of negative ions is smaller than that for the positive ions (cf. Chapter 3, section 3.5).
- Most experimental results show that when corona stabilisation occurs, the initial current pulse is large indicating a large initial streamer corona. For this reason, an initial model may consider only the initial streamer.

Chapter 6. Quantitative Modelling of Breakdown under Corona Stabilisation

It is apparent from the foregoing discussions presented in previous chapters that the breakdown process comprises of complex and interwoven physical processes dependent on a large number of parameters. An approach is presented here whereby approximate relationships between defect characteristics and discharge events are used to provide an order of magnitude estimate model. Only the partial discharge and the inception of the leader is considered in this model. However, we initially concentrate on small gaps where the leader stepping process is less significant and the leader inception voltage is very close to the breakdown voltage.

6.1 Approach To Quantitative Modelling

The model presented here is for the geometry of a particle defect rather than a laboratory-style point-to-plane. The case of a conducting particle placed in a background electric field is technically more significant than a point to plane laboratory setup. One of the main factors limiting the operating stress of GIS equipment is particle contamination which can reduce the insulation level by as much as 90 percent [58]. Furthermore, one of the primary uses for a model would be identification of the particle in the context of GIS diagnostics. Thus a model relating the particle characteristics to measurable discharge parameters would be very useful. The approach to modelling breakdown from a particle defect used here is to break the discharge into its sub-processes. Those sub-processes that have less significant effects are simplified or neglected in this first-order accuracy approach. For the processes that are believed to have greater significance, the most accurate theoretical or semi-empirical calculations used by other researchers in other models have been researched and used where appropriate.

6.2 Geometry Used

The geometry used is that of a fixed conducting particle defect in a uniform background field. The particle is characterised by its length and radius as shown in *Figure 6.1*, where L_p is the particle length, r_p the particle radius and E_0 the applied background field.

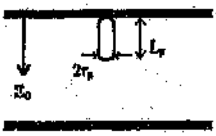

Figure 6.1: Particle In Uniform Field

6.3 Method Of Modelling

The calculations for each stage of the modelling process are discussed in this section. *Figure 6.2* presents the model in flow-diagram form. The discussion that follows may be read in conjunction with the flow-diagram in *Figure 6.2*.

6.3.1 Applied Stress

The applied waveform may be taken as a.c., in which case the peak charge contained in the discharge at the peak of the voltage waveform may be calculated as in [56,59]. Or the model may be adapted so that the values of U_0 (and thus E_0) may increase in time according to some slow-rising applied waveform. For example, according to Rong et al [60], there is a 100% probability of stabilisation if the steepness of the applied impulse is smaller than 5kV/μs, therefore using time steps of 1μs and increasing U_0 by 5kV each time step could be a method used.

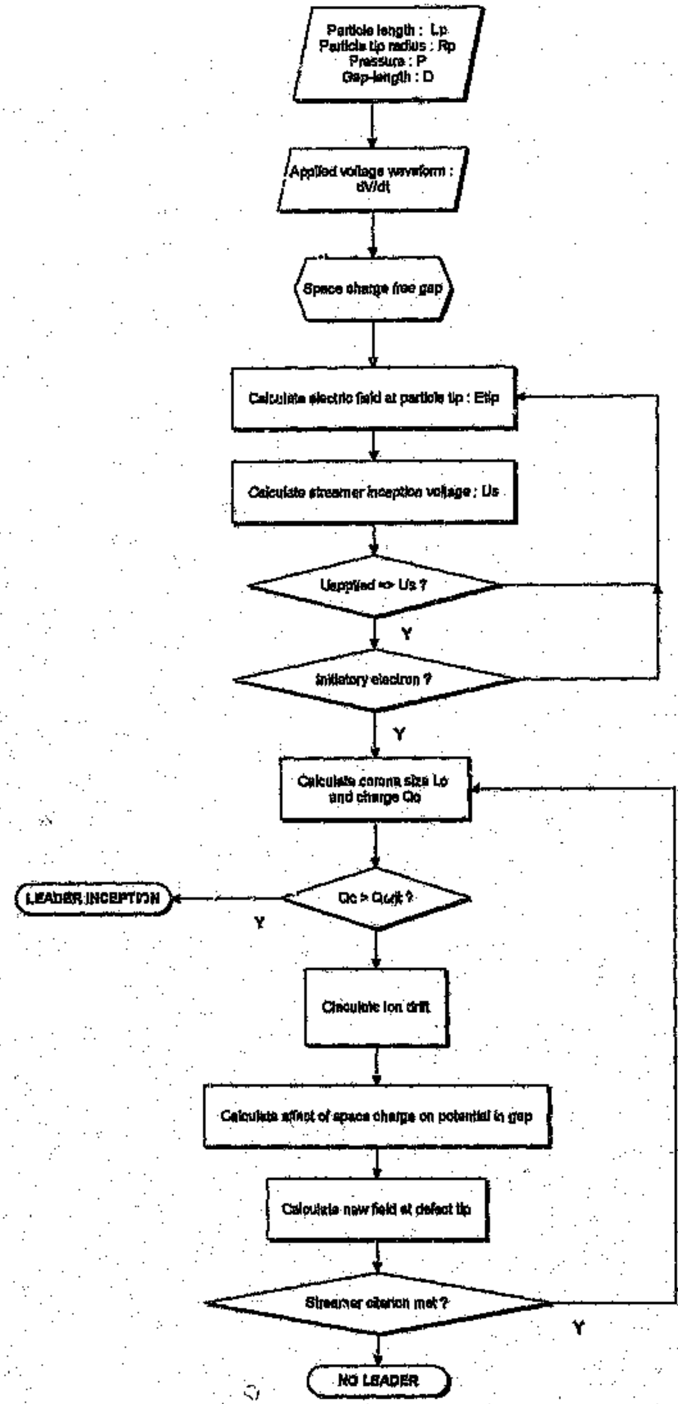

Figure 6.2: Flow Diagram For Leader Inception Calculation

6.3.2 Electrode Geometry

If a point-plane geometry is used, it is necessary to use some numerical calculation method to determine the electric field magnitude at the point. In the case of a particle in a background electric field, it is possible to derive an analytical expression for the field intensification caused by the particle. Cooke [61] has derived an expression to calculate the electric field at the tip of a particle of length L_p and a hemispherical tip of radius r_p. Equation (6.1) gives the electric field magnitude, E, at a radius x from the center of the hemispherical tip of the particle with the applied background field E_0.

$$E = E_0\left[1+\left(\frac{L_p}{2r_p}\right)\frac{4r_p^2}{4x^2}+\frac{\left(2r_p\right)^3}{4x^3}\right] \tag{6.1}$$

6.3.3 Streamer Inception

To calculate the voltage at which streamer inception occurs, the well known Nitta-Shibuya formula (equation (6.2)) may be used [44].

$$U_{st} = \left(\frac{E}{p}\right)_{cr} p\frac{\left(1+\frac{a}{\sqrt{pR}}\right)^2}{\left(\frac{E}{U}\right)_{max}} \quad , a \approx 2{,}783 \text{ Pa}^{1/2} m^{1/2} \tag{6.2}$$

(R is the rod-radius)

This equation was however conceived for point to plane geometries. A method of determining inception in the case of a particle defect is derived in [59] :

$$U_{st} = \frac{\left(\frac{E}{p}\right)_{cr} pF\left[\left(pL_p\right),\left(\frac{L_p}{r_p}\right)\right]}{\frac{E_0}{U_0}} \tag{6.3}$$

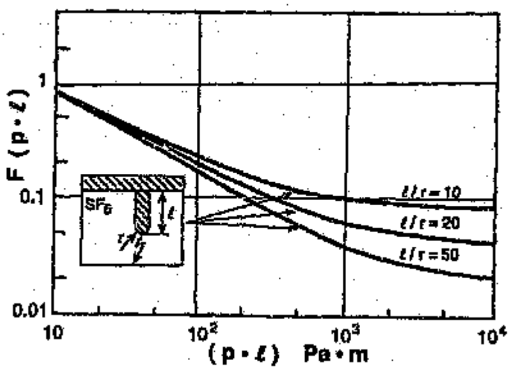

Figure 6.3 Streamer inception function F in dependence of *(p.l)* from [59]

The ratio E_0/U_0 is the reduced background field at the defect location (in the absence of the defect). F is a dimensionless streamer inception function which is obtained by reducing the well known critical avalanche streamer inception criterion to a general form, the details of this are given elsewhere [59]. For a given defect (i.e. defined by aspect ratio L_p/r_p), F is dependent on the product pL_p. Curves plotting the function F in dependence of pL_p for various L_p/r_p ratios are given in [59] (see *Figure 6.3*).

From equation (6.3) it can be seen that the measured inception voltage provides information (at a known pressure) about the particle's physical characteristics, length and aspect ratio, as well as the reduced background field at the particle location. This could be useful for GIS diagnostics.

6.3.4 First-Electron Delay

The measured streamer inception voltage for increasing waveforms of positive polarity is invariably larger than that predicted by the streamer criteria. This is mainly due to first electron delay. The initial electron needed to start an avalanche is, in SF_6, believed to be provided by field-induced detachment from negative ions created in the ambient gas by cosmic radiation [5]. The probability of the "first" electron being made available for an avalanche and of the avalanche surviving to reach streamer size has a significant effect on the streamer inception and breakdown voltages. There have been a few attempts to describe this probability mathematically, detailed accounts of which may be found in [5] and [62]. Wiegart et al [5] have produced an approximation for the first electron delay which takes into consideration factors such as the equilibrium ion concentration in the virgin gas, the influence of the electric field and electrode geometry on the ion concentration as well as the field dependent detachment process. The approximate time lag may be calculated using a modified volume-time law [5]:

$$P(t)=1-e^{\left\{-\int_0^t \int_{Vcr} \frac{dne}{dt}\left(1-\frac{\alpha}{\eta}\right)dVdt\right\}} \tag{6.4}$$

The integration in space in (6.4) is done over the critical volume (V_{cr}) . dn_e/dt is the electron production rate, the calculation of which is not a trivial problem, but simplifications are given in [5].

6.3.5 Corona Length

We will assume a hemispherical distribution of charge in space around the defect. The radius of this distribution will be necessary to calculate the potential difference due to the space charge. Once the first streamer corona has formed and reached its maximal length, the positive ions are distributed at the boundary of the corona. We need to calculate the distance drifted by these ions towards the opposite electrode in order to work out the radius of the space charge distribution. The approximate radius will thus be given by the sum of the radius of the first corona boundary and the distance drifted by the ions in a given time.

The mobility of positive ions is given by equation (6.5) below [5] :

$$\mu_+ = \mu_+^0\left(\frac{p_0}{p}\right)\left(\frac{T}{T_0}\right) \tag{6.5}$$

$$\approx 5\text{x}10^{-5}\frac{m^2}{Vs}.\frac{760\text{x}1{,}33\text{x}10^2\,Pa}{p}\frac{T}{273{,}16K} \tag{6.5.1}$$

assuming an ambient T of about 300K,

$$\mu_+ \approx 6\frac{m^2}{Vs}.\frac{1}{p} \tag{6.6}$$

The drift velocity is therefore :

$$v_{d+} \approx \mu_+.E \approx 6\frac{m^2}{Vs}.\frac{E}{p} \tag{6.7}$$

The distance covered by the ions in time t is thus :

$$L_{drift} = v_{d+} \cdot t \tag{6.8}$$

As an approximation, the corona length may be taken as the length of the longest streamer which is given in [17] :

$$L \approx C_l\left(\frac{U}{E_{cr}}\right) \tag{6.9}$$

where C_l is approximately = 0.5

The radius of the positive ion distribution is therefore approximately equal to $L_{drift} + L$, i.e.

$$L_{total} = L_{drift} + L \tag{6.10}$$

6.3.6 Corona Charge

The charge in the initial corona structure can be calculated using the method described in [59], where the true charge deployed by the initial discharge has been derived to be approximately given by :

$$q_1 \approx \frac{\pi\left(L_p \cdot E_0\right)^2}{\left(\frac{E}{p}\right)_{cr} \cdot p} \tag{6.11}$$

This equation for charge arises from a more complicated expression derived in [59] by considering the space charge distribution to be in the shape of an ellipsoid (the positive space charge deployed ahead of the protrusion induces a mirror negative charge in the electrode). The approximate assignment of ellipsoidal axes is shown in *Figure 6.4*.

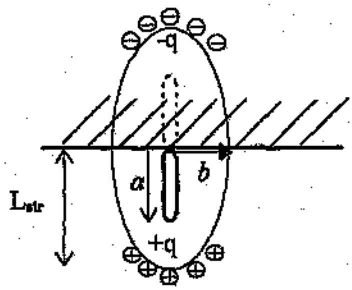

Figure 6.4 : Equivalent ellipsoidal axes a and b

The charge deployed in a partial discharge is given by a dimensional relationship between the defect length, the potential difference due to the discharge and a dimensionless proportionality factor which accounts for the charge distribution. The details of deriving this form of charge calculation are given in [59], only the equations are reproduced here :

The equation for the true charge deployed is

$$q = \pm g.\pi.\varepsilon_0.L.\Delta U \tag{6.12}$$

and the dimensionless proportionality factor g is given by

$$g = \frac{1}{2}\frac{a/L}{(a/b)^2}\left[1+\varepsilon_r\left(K(a/b)-1\right)\right] \tag{6.13}$$

where a and b are the approximate axes of the ellipsoid and K is a dimensionless function of a and b. K is approximately 3 for a oblate ellipsoid and is about equal to 4a/b for prolate ellipsoids [59].

The potential due to the space charge is then

$$\Delta U_{qs} = \frac{q_s}{g\varepsilon_0 L} \tag{6.14}$$

g can be calculated from (6.13) where a is approximately equal to the defect length, and b equal to the streamer length [59]. We can replace the b by the streamer length plus the distance drifted by the ions as calculated by equation (6.10). q_s is the true charge injected by the first corona , q_1.

6.3.7 Second Corona Charge

There are two contributions to the enhanced field (driving the partial discharge) at the defect. The applied voltage which is the enhancement of the background field E_0 by the defect, as well as the effect of space charge. These two contributions can be integrally expressed by the potential differences they cause over the gap. This is expressed in equation (6.15) :

$$\Delta U = \Delta U_a + \Delta U_q \qquad (6.15)$$

ΔU is the potential difference available across the gap to drive the discharge. ΔU_a is due to the enhanced applied field. ΔU_q is given by equation (6.14) above. Whereas in the calculation of the first streamer corona (space charge free) the contribudion of ΔU_q is neglected, the calculation is repeated for the second corona with thc potential due to the space charge from the previous discharge included. A new value for injected charge, q_2, can now be calculated by using the same method as for the space-charge free case but with a new value of potential difference (and electric field) corrected for the space charge potential difference.

6.3.8 Critical Charge

Wiegart et al [5] have determined a leader-inception criterion based on th amount of charge injected by an impulsive streamer corona. Once a critical value of charge is exceeded, there is sufficient energy to allow leader formation. This criterion is simplified into an equation suitable for use in a model

$$Q_{cr} = 45nC\left(\frac{p}{100kPa}\right)^{-2.2} \qquad (6.16)$$

If the second corona charge q_2 is greater than Q_c , then the leader inception criterion has been met. If this condition is not met, the calculation method should be repeated with the new space charge q_2.

6.3.9 Model Implementation

The model was implemented in the C++ language using the Microsoft Visual C++ 4.0 compiler, using the Microsoft Foundation Classes. The application was written with a simple dialog-box based interface where the user is prompted to enter the relevant data describing the geometry and input waveform (see *Figure 6.5*). The "Simulate" push-button runs the simulation. The results of the simulation are then presented in a dialog box. The full source code has been included in Appendix C.

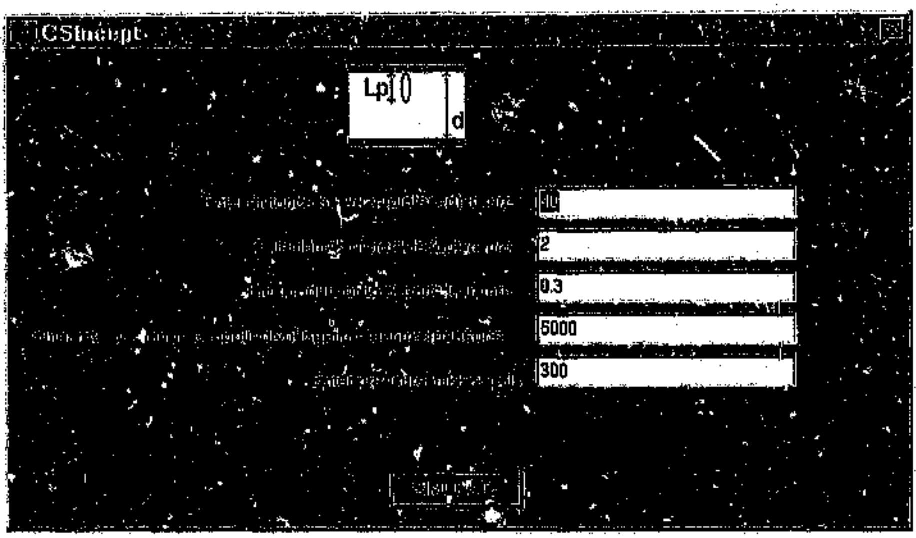

Figure 6.5 User Interface to Program

6.4 Results and Discussion

Since breakdown under fast impulses has already been accurately modelled, the first implementation of the model neglects initiatory electron delay (since the probability of a first electron under slow impulses has been found to be virtually 1 [8]). There is great difficulty in verifying the model, since there are very few published experiments that measure the variables of interest for this specific geometry and at variable voltage steepnesses. Rong et al [60] presented a paper describing experimental work looking at the influence of voltage steepness on breakdown from a small needle defect fixed on one electrode in a quasi-uniform field (the point defect was fixed on a spherical electrode). Results in [60] were presented for a nichrome wire of 2mm length and 0,3mm diameter at a pressure of 300kPa and electrode-separation of 40mm. These values were thus used in the simulation. The experiments in [60] were performed at numerous applied voltage steepnesses, the simulation is thus run at a number of the slower impulses (since this would test the corona-stabilisation aspect of the model).

6.4.1 Time to breakdown

Only one breakdown time measurement is published in [60].

Measured Breakdown Time for dV/dt=10kV/μs =	43μs
Predicted Breakdown Time for dV/dt=10kV/μs =	37μs

Table 6.1 Time to Breakdown Result

6.4.2 Breakdown Voltage vs. dV/dt

The relationship between breakdown voltage and dV/dt is plotted in [60].

The measured values for the slow waveforms are :	The predicted values are :
$V_{breakdown}$ @ 5kV/μs = 480kV	$V_{breakdown}$ @ 5kV/μs = 372kV with $t_{breakdown}$ = 70μs
$V_{breakdown}$ @ 10kV/μs = 500kV	$V_{breakdown}$ @ 10kV/μs = 375kV with $t_{breakdown}$ = 37μs

Table 6.2 Breakdown Voltages at Two dV/dt values

6.4.3 Influence of various needle lengths

The breakdown voltages at a voltage steepness of 1.56kV/μs and at various needle lengths (from 1 to 5mm) are measured in [60]. Note that in the case of varying needle lengths, the dimensionless streamer inception function F (cf. Section 6.3.3) will differ for each length.

Lp=	Measured V=	Predicted V=
1mm	500kV	460kV
2mm	450kV	390kV
3mm	400kV	350kV
4mm	400kV	350kV

Table 6.3 Influence of Needle Lengths

6.4.4 Discussion of results

The breakdown time predicted for the 10kV/μs waveform compares very well to the measurement. Also, when moving to a slower waveform (eg.5kV/μs) the time to breakdown increases (as expected). The predicted breakdown magnitudes are smaller than those measured (but in the same order of magnitude). This is because the simulation used only tracks the growth and effect of the space charge from the initial streamer corona. The secondary avalanches (discussed in chapter 5) contribute to the higher breakdown voltage measured experimentally. However, in [60], a plot of breakdown voltage versus dV/dt shows that the breakdown voltage increases only slightly from 2kV/μs to 20kV/μs. This trend also occurs in the simulation.

The breakdown voltages predicted for various needle lengths (at the same applied dV/dt) are also smaller than those measured. However, again the measurements show a trend of the breakdown voltage flattening out as needle length increases, this trend occurs in the simulation.

Chapter 7. The Problem of True Charge Measurement and the Design of a Suitable Experimental Setup

In the preceding chapter, a method of modelling breakdown in SF_6 was presented for the geometry of a fixed conducting particle defect in a uniform background field. In this chapter, the difficulty of measuring the true charge deployed in a discharge for a conventional point to plane arrangement is theoretically explained. There is difficulty in refining and improving the model presented in Chapter 6 because most published results are based on conventional experimental setups. Based on the theory presented here, an experiment is described that simulates a particle defect geometry *and* allows measurement of the true charge deployed in the discharges at the defect.

7.1 Measuring True Charge Injected into a Partial Discharge

In partial discharge detection experiments, the charge deployed in the discharge is often taken to be the time integral of the current flowing in the lead attached to the measuring electrode. This current has in fact two components, the conduction current due to the actual charge injected in the discharge and a displacement current. It is shown that it is difficult to isolate the two components in the measured current. This analysis holds only in the absence of polarisable materials in the interelectrode space, therefore the definition of polarisation is also presented as part of this theory. An experimental configuration is presented whereby an accurate value for conduction current may be measured by minimising displacement current. This experiment has the specific goal of measuring the true charge in a partial discharge from a fixed particle defect placed in a uniform field. The theory presented here provides justification for the experimental arrangement [63].

7.2 Polarisation

In dielectrics, conduction occurs when an applied field sets charges in motion and this motion may continue as long as the field is applied. In some materials this motion may be hindered or stopped completely, i.e. the charges may be trapped in the material. The effects due to the hindering of the motion of charges in the dielectric are collectively known as polarisation. The *polarisation vector* is defined as :

$$\mathbf{P} = \mathbf{D} - \varepsilon_0 \mathbf{E} \qquad 7.1$$

where the E is the electric field, ε_0 the permittivity of free space and the *electric displacement vector* or *electric flux density vector* is given by :

$$\mathbf{D} = \varepsilon \mathbf{E} \qquad 7.2$$

In SF_6 the permittivity of the medium is equal to that of free space so that the polarisation is equal to zero.

7.3 The Relationship between Charge and Voltage between Space Charge Free Electrodes

Consider a parallel plate configuration as in the figure below :

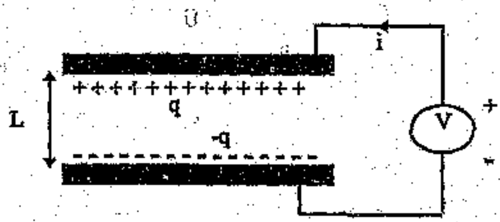

Figure 7.1 : Parallel Plates (no space charge)

The electric field between the plates is

$$\mathbf{E} = \frac{\mathbf{V}}{\mathbf{L}} \qquad 7.3$$

The charge on the upper plate is given by Gauss' Law:

$$q = \iint \mathbf{D} \cdot d\mathbf{A} = \varepsilon_0 E A \qquad 7.4$$

Thus the relationship between charge and voltage is

$$q = \frac{\varepsilon_0 A}{L} V \equiv CV \qquad 7.5$$

This capacitance relationship is linear and holds strictly true only in a vacuum - if anything is placed between the electrodes, the fields will change, along with the charge on the electrodes. The charge on the electrodes in the absence of space charge is thus given by equation 7.5 .

7.4 Conduction Current and Displacement Current

Consider the current flowing to an electrode as follows :

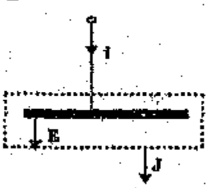

Figure 7.2 : Current flow to an electrode

Applying charge conservation for the volume enclosing the electrode, the current is given by :

$$i = \iint \mathbf{J} \cdot d\mathbf{A} + \frac{\partial q}{\partial t} \qquad 7.6$$

Using Gauss' Law (i.e. $q = \oint\!\!\oint \mathbf{D} \cdot d\mathbf{A}$) and substituting for q, we get :

$$i = \iint \left(\mathbf{J} + \frac{\partial \mathbf{D}}{\partial t} \right) \cdot d\mathbf{A} \qquad 7.7$$

The conduction current is **J**, and the displacement current $\partial \mathbf{D}/\partial t$. Note that without information about charge motion in the electrode vicinity it is impossible to separate the two components of the current measured in the external circuit.

7.5 Current Flowing in the Measurement-Electrode Lead During a Discharge

Consider a pair of electrodes containing a gaseous dielectric to which a voltage is applied that leads to a discharge in the interelectrode space.

In the absence of space charge, the charge on the electrodes is given by

$$q_c = CV \tag{7.8}$$

as derived earlier (equation 7.5). The "capacitive" current is thus :

$$\frac{dq_c}{dt} = C\frac{dV}{dt} \tag{7.9}$$

The current due to charge induced on the electrode by space charge is

$$\frac{dq_s}{dt} \tag{7.10}$$

The total current as measured at the measurement electrode is given by :

$$I = I_t + \frac{dq'}{dt} \tag{7.11}$$

Where I_t represents the true charge transferred to the discharge and q' is the total charge on the electrode :

$$q' = q_s + q_c = q_s + CV \tag{7.12}$$

Therefore ,

$$I = I_t + \frac{dq_s}{dt} + C\frac{dV}{dt} \quad 7.13$$

An infinitesimal charge dQ in the inter-electrode space will induce a charge dq_s on the electrode. This induced charge will be proportional to dQ from the superposition principle, i.e.

$$dq_s = -\phi dQ \quad 7.14$$

where ϕ is a dimensionless scalar function which depends on the location of dQ only. To get the total induced charge the following volume integral needs to be calculated :

$$q_s = -\iiint \phi\rho \, d\Omega \quad 7.15$$

Where ρ is the volume charge density at the location of the volume element Ω . The volume is evaluated over the entire inter-electrode volume. In the absence of polarizable materials, ϕ is given by

$$\nabla^2\phi = 0 \quad 7.16$$

With the boundary conditions $\phi = 1$ at the surface of the measuring electrode and $\phi = 0$ at the other electrode. Differentiating equation 15 gives :

$$\frac{dq_s}{dt} = -\iiint \phi \frac{\partial\rho}{\partial t} d\Omega \quad 7.17$$

And by substituting for $\partial\rho/\partial t$ from the continuity equation :

$$\nabla \cdot J + \frac{\partial\rho}{\partial t} = 0 \quad 7.18$$

we get

$$\frac{dq_s}{dt} = -\iiint \phi \, \nabla \cdot \mathbf{J} \, d\Omega \qquad 7.19$$

or , since ϕ is a scalar field ,

$$\frac{dq_s}{dt} = \iiint \nabla \cdot (\phi \mathbf{J}) \, d\Omega - \iiint \mathbf{J} \cdot \nabla \phi \, d\Omega \qquad 7.20$$

Applying Gauss's Divergence Theorem to the volume integral of the divergence of $\phi\mathbf{J}$, given that ϕ is 1 at the measuring electrode and zero at all other electrodes ,

$$\mathbf{I}_t = -\iiint \nabla \cdot (\phi \mathbf{J}) \, d\Omega \qquad 7.21$$

Inserting equations 7.21 and 7.20 into equation 7.13 , the expression for the current flowing into the lead is :

$$\mathbf{I} = -\iiint \mathbf{J} \cdot \nabla \phi d\Omega + C \frac{dV}{dt} \qquad 7.22$$

It is apparent from this expression that the current due to actual charge transfer into the discharge I_t cannot be solved for since it is implicit in this equation. It can be deduced from this equation that *the charge transferred to the gap from the electrode contributes to the current in the lead connected to the electrode only by the charge-induction effects that occur when these charges move in the interelectrode space.*

7.6 Charge Measurement

In partial discharge measurements, the current in the lead is integrated to provide a value of charge. Thus if we integrate equation 7.13 :

$$Q_{measured} = CV + Q_t - \iiint \phi \rho \, d\Omega \qquad 7.23$$

Q_t represents the charge transferred into the discharge. Q_t will be equal to the net charge in the interelectrode space if no charge has been added to or lost from the gap at other electrodes, that is

$$Q_t = \iiint \rho \, d\Omega \qquad 7.24$$

In this case, equation 7.23 can be written as :

$$Q_{measured} = CV + \iiint (1-\phi)\rho \, d\Omega \qquad 7.25$$

From equation 7.23 it is clear that the measured charge *cannot* be said to be just the sum of the capacitive charge and transferred charge - in order for this to be true, in the induced charge term the volume integral of $\phi\rho$ be zero (which would only occur if a quantity of charge equal to the transferred charge left the gap via other electrodes).

7.7 Experiment to determine True Charge Transferred from a Fixed Point Defect in a Uniform Field

The difficulties involved in separating the displacement current\charge from the conduction current\charge has been explained in the preceding sections. In order to circumvent these problems *for a specific geometry* , the following experiment is useful [56] :

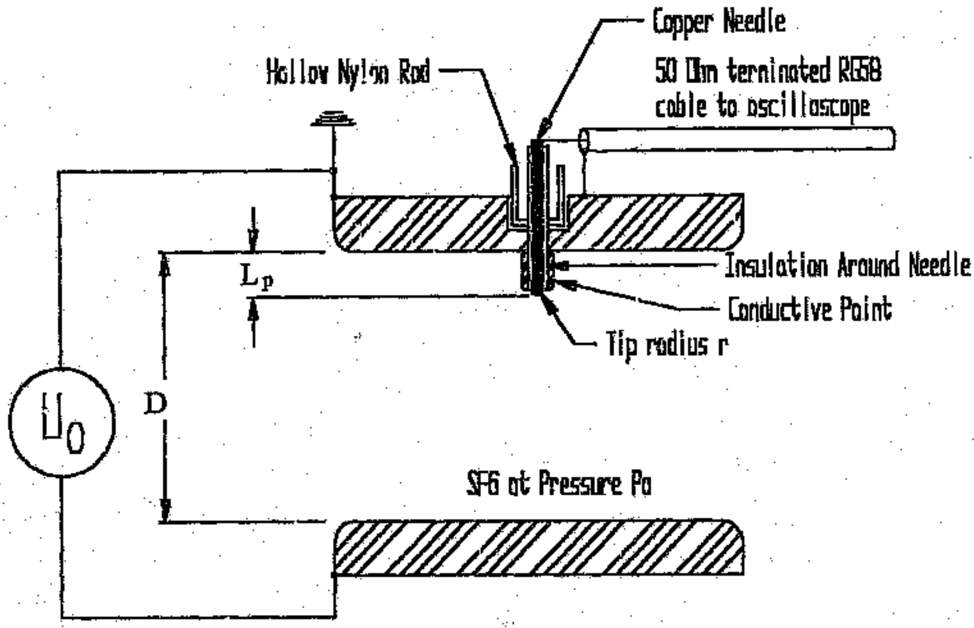

Figure 7.3 ; Experimental setup schematic (not to scale)

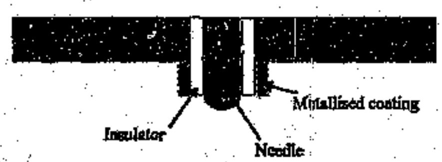

Figure 7.4 : Exaggerated view of upper electrode

In this setup, the aim is to simulate the behaviour of a needle defect fixed at one electrode in a uniform field. The needle is coated with a layer of insulation except for its tip and the outside of the insulating layer is metallised. The metallised layer is in contact with the plate electrode. The protrusion is then connected to an oscilloscope. The needle is thus the measuring electrode. If we rewrite equation 7.13 here:

$$I = I_t + \frac{dq_s}{dt} + C\frac{dV}{dt}$$

it can be seen that the CdV/dt component is very small, since no voltage is directly applied to the needle. Although the capacitance involved may be small, the fast rise times involved in the corona pulses may give rise to displacement current that will flow between the needle an the top plate, but this current can be calculated and subtracted from the measured current (the capacitance formed between the needle and upper plate is a well defined coaxial cylinder capacitor, the value of which can be easily computed). This final current will therefore be very close to I_t (the current due to the charge transferred to the gap from the needle). Integration of this current thus gives a good estimate of the charge deployed in the partial discharge from the needle.

Chapter 8. Conclusion

This final chapter reviews the work presented in this thesis. Some final conclusions are drawn and recommendations are made as to what further work is considered to be most beneficial.

8.1 Summary

- Chapter 1 presented the background to this study and set out the objectives to be met. Terminology that is commonly used ambiguously was clarified.
- In Chapter 2, the state of the art theory of positive lightning impulse inhomogeneous-gap breakdown in SF_6 was expounded. This was necessary since the leader-precursor theory must also operate under slow rising impulses (switching impulses, for example) where corona stabilisation occurs.
- In Chapter 3, an analysis was made of the methods currently available to theoretically model discharges. The ideal quantitative model of corona stabilised discharge would be a theoretical model which could be applied over a wider range of conditions than an empirical or semi-empirical method of prediction. The conclusion of this analysis is that none of the methods are currently able to model the complete corona stabilised breakdown process. Also, the results of some theoretical and numerical simulations of SF_6 discharges that are germane to an understanding of ion-drift stabilisation were discussed.
- In Chapter 4, relevant empirical studies were detailed. The empirical observations noted here formed a framework for building a theory of the mechanism whereby ion drift corona stabilised discharge/breakdown occurs.
- In Chapter 5 a qualitative model was presented based on the analyses discussed in previous chapters. In particular, the random pulse-burst nature of positive impulse breakdowns was explained and a semi-hemispherical (or ellipsoidal) space charge distribution model was justified.
- A quantitative model to predict leader inception under slow rising positive voltages from a fixed particle defect placed in a uniform background electric field was presented in Chapter 6. A comparison of the results of the model to a published set

of measurements was favourable and thus indicates that the approach presented here is feasible to model corona stabilised breakdown.

- Chapter 7 presented a theoretical proof that the current (and charge) measured at the electrodes in a conventional point to plane experiment does not allow one to determine the true charge deployed in discharges. An experiment was designed to allow for measurement of true charge in an arrangement that simulates a fixed particle defect in a uniform background electric field.

8.2 Recommendations

One of the chief features of the model in Chapter 6 is that it allows one tc describe the input voltage in terms of the steepness of the impulse (i.e. the dV/dt). Using the experimental arrangement of Chapter 7, the charge deployed in discharges as a function of various dV/dt's may be measured. The correlation with theory should allow for refinement of the model.

Hidaka [64] has developed an optical technique to measure the actual field due to space charge. Hidaka uses a Pockels Sensor as a probe to measure electric field strength. The advantage of a Pockels sensor over conventional probes is that the electric field distribution is disturbed only marginally. The figures below show how Hidaka applied the sensor to measuring electric field distribution directly in a point to plane discharge in air. Using this sensor with the experimental setup of Chapter 7 would provide invaluable information about the actual distribution of space charge in an SF_6 discharge.

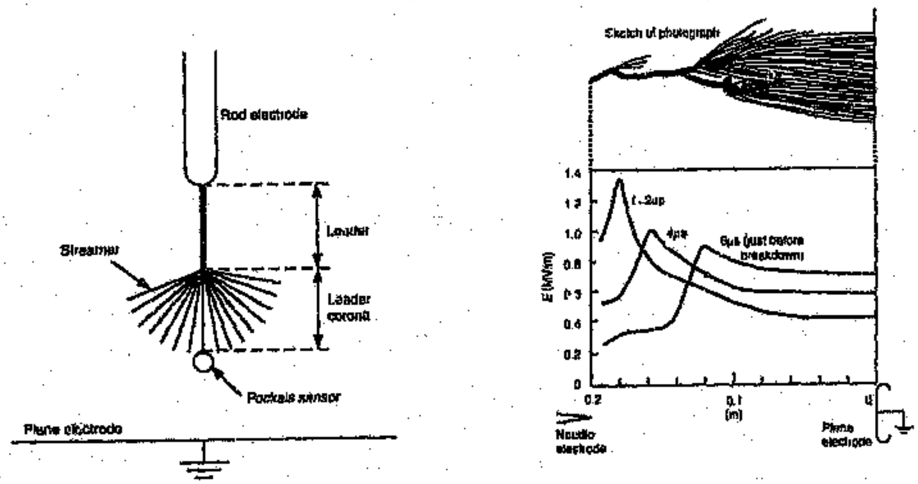

Figure 8.1 Use of a Pockels Sensor to measure electric field distribution in the breakdown of an air gap stressed by positive lightning impulse voltage [64]

This dissertation has presented a comprehensive evaluation of methods available to predict the effect of positive ion drift on breakdown/discharge in SF_6. Empirical investigations relevant to this phenomenon were also detailed and a theory of corona stabilised breakdown was forged from studying the empirical and simulation data presented. A quantitative model of first-order accuracy was designed to predict corona stabilised breakdown. The methodology followed in this model was to select the optimal calculation or approximation f · each stage of the discharge process. These selections were justified by the results of other theoretical models and experimental observations. The results of a first implementation of the model compare very favourably to published results thus reinforcing the assertion that the method presented here is currently the most beneficial approach to modeling corona stabilisation.

APPENDIX A : Derivation of the Boltzmann Transport Equation

According to the kinetic theory, the molecules of a given gas have velocities ranging from zero to infinity and their average velocity is constant with constant temperature and pressure. Therefore, in many applications we consider all the gas particles to be moving at some average velocity. In a more rigorous analysis of gaseous plasma it becomes necessary to take the distribution of velocities of all the particles into account. In addition, each particle also has a position in three dimensional space that has to be accounted for. Therefore two three-dimensional vectors are needed to describe each particle in terms of both its velocity and position. The x, y and z coordinates describing the position of the particle are said to be in the *physical space* and the three components of the velocity vector are part of the *velocity space*. If a coordinate system is defined in terms of six coordinates - three for position and three for velocity - then such a system is called the *phase space*. For a collection of N particles, we thus need to know 6N coordinates. The mathematical relation which specifies the phase space distribution function of a collection of particles is called the Boltzmann equation. This equation is derived as follows :

Consider a gas with particles of mass m, velocity distribution given by function f, and $m\gamma$ an external force acting on each particle. Assuming negligible interaction at large distances among the particles, the number of particles occupying a volume is :

$$dV = dx\, dy\, dz\, dv_x\, dv_y\, dv_z \tag{1}$$

in phase space at any instant t is given by

$$\left(\frac{dn}{n}\right)_t = f(\mathrm{r} + \mathrm{v}dt, \mathrm{v} + \gamma\, dt, t)\, dV \tag{2}$$

where the vector **r** has the coordinates x, y, and z and the vector **v** the coordinates v_x, v_y and v_z. In a time interval dI, these molecules will be displaced by **v**d*t* and their velocities will be altered by γd*t*.

If it is assumed that during this time interval these particles did not undergo any collisions, their number

$$\left(\frac{dn}{n}\right)_{t+dt} = f(\mathbf{r}+\mathbf{v}\,dt,\ \mathbf{v}+\gamma\,dt,\ t+dt)\,dV \qquad (3)$$

would remain unchanged. However, because of collisions with other particles in the remainder of phase space, some of the molecules in d*V* will be removed from it by modifying either the speed or position. At the same time, other particles that have not been in d*V* at time *t* will undergo collisions during d*t*, thus acquiring the same position in phase space as our assembly. The variation in the number of these particles during the interval d*t* is obviously proportional to d*V* and dt. If we call the constant of proportionality $(\partial f/\partial t)_c$, the change in the number of molecules will be given by the difference,

$$\left(\frac{dn}{n}\right)_{t+dt} - \left(\frac{dn}{n}\right)_{t+dt} = \left(\frac{\partial f}{\partial t}\right)_c dV\,dt \qquad (4)$$

and inserting values from the right hand sides of (2) and (3) into (4) , we get

$$\left[f(\mathbf{r}+\mathbf{v}\,dt,\ \mathbf{v}+\gamma\,dt,\ t+\mathrm{d}t) - f(\mathbf{r},\mathbf{v},t)\right] dV = \left(\frac{\partial f}{\partial t}\right)_c dV\,dt \qquad (5)$$

Expanding the first term on the left-hand side by Taylor's series, we get

$$f(\mathbf{r},\mathbf{v},t) + \mathbf{v}\,dt\,\frac{\partial f}{\partial \mathrm{r}} + \gamma\,dt\,\frac{\partial f}{\partial \mathrm{v}} + dt\frac{\partial f}{\partial \mathrm{t}} - f(\mathbf{r},\mathbf{v},t) = \left(\frac{\partial f}{\partial \mathrm{t}}\right)_c dt \qquad (6)$$

from which follows

$$\frac{\partial f}{\partial \mathrm{t}}+\mathrm{v}\frac{\partial f}{\partial \mathrm{r}}+\gamma\,\frac{\partial f}{\partial \mathrm{v}}=\left(\frac{\partial f}{\partial \mathrm{t}}\right)_c \tag{7}$$

which is the Boltzmann (transport) equation.

APPENDIX B: Derivation of the Continuity Equation

Consider a volume of space within which charged particles interact. Let us consider only one particular species of charge.

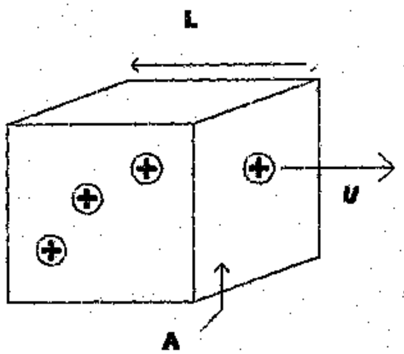

Figure B.1 A volume in space with moving particles

Strict conservation of charge is not of concern here - since only one species of charge is considered, charge may be "created" (for example electrons may be created by ionisation) or charge may be "destroyed" (when electrons recombine with positive ions, for instance).

Therefore, for a particular species of charge in a particular volume of space, particles may be generated by certain mechanisms, they may diminish through recombination and there is also motion of particles across the boundary surfaces of the volume of space.

The net increase of particles in a particular volume is then :

$$\text{net increase} = \text{generation} - \text{recombination} - \text{loss through sides} \qquad (1)$$

If the number density of particles (particles per m^3) is n and the volume of the region in space is V :

$$rate\ of\ net\ increase = \frac{\partial}{\partial t}\iiint n\, dV \qquad (2)$$

If the volume is kept fixed in space, the derivative can be taken inside the volume integral :

$$rate\ of\ net\ increase = \iiint \frac{\partial n}{\partial t}\, dV \qquad (3)$$

Generation and recombination can be handled similarly, using the volume generation rate (G particles per cubic meter per second) and volume recombination rate (R particles per cubic meter per second).

The last term in equation 1 is the net loss through the sides of the enclosing surface. This can be written as the integral of the outward particle flow over the enclosing surface as :

$$loss\ through\ sides = \oint\!\!\oint \Gamma \cdot d\mathbf{A} \qquad (4)$$

The quantity Γ is called the particle flux vector. It points in the direction of particle movement and its magnitude is given by the number of particles passing a unit area in a second. As an example, consider the surface as a parallelpiped with a length l and area A filled with particles with a density n all of which are moving to the right with a velocity u. In a time $t=l/u$ all of the particles will pass through the end area, a total of nAl particles. The flux of particles is then :

$$\Gamma = \frac{nAl}{(l/u)A} = n\mathbf{u} \qquad (5)$$

If the particles each have a charge q, the current density is given by

$$\mathbf{J} = q\Gamma \qquad (6)$$

The conservation equation for an individual species, equation 1 can now be written in terms of these integrals as:

$$\iiint \frac{\partial n}{\partial t} dV = \iiint G\, dV - \iiint R\, dV - \oiint \Gamma \cdot d\mathbf{A} \tag{7}$$

when the surface is fixed.

The flux integral is a surface integral, whereas all of the other integrals in the particle conservation equation are volume integrals. We can convert the area integral by using Gauss' theorem as:

$$\oiint \Gamma \cdot d\mathbf{A} = \iiint (\nabla \cdot \Gamma) dV \tag{8}$$

Since all of the integrals are now taken over the same fixed volume, the particle conservation equations may be written in terms of the integrands alone as:

$$\frac{\partial n}{\partial t} + \nabla \cdot \Gamma = G - R \tag{9}$$

This is a common form of the equation. It may be re-written in other forms accounting for specific generation and recombination methods of particular species of charge.

APPENDIX C :Source Code for CSINCEPT Program

The complete source code for the implementation of the model in Chapter 6 is included in this appendix. Except for any bitmaps, which are non-essential to the functioning of the model, the information included here will allow for a complete re-construction of the program.

C.1 Class Information

The classes used are shown in *Figure C.1* below :

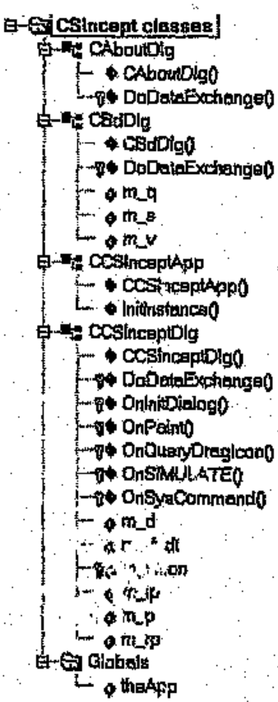

Figure C1 : Class Information Diagram

C.2 List of Files

The filenames of the files printed out in the following pages are :

.cpp source files :
CSIncept.cpp
CSInceptDlg.cpp
BdDlg.cpp
StdAfx.cpp

.h header files
CSIncept.h
CSInceptDlg.h
BdDlg.h
StdAfx.h
Resource.h

Other Files :	
CSIncept.mak	(Project Make file)
CSIncept.clw	(Class Wizard Information File)
CSIncept.rc	(Resource Script)

CSIncept.cpp

```
// CSIncept.cpp : Defines the class behaviors for the application.
//

#include "stdafx.h"
#include "CSIncept.h"
#include "CSInceptDlg.h"

#ifdef _DEBUG
#define new DEBUG_NEW
#undef THIS_FILE
static char THIS_FILE[] = __FILE__;
#endif

/////////////////////////////////////////////////////////////////////////////
// CCSInceptApp

BEGIN_MESSAGE_MAP(CCSInceptApp, CWinApp)
	//{{AFX_MSG_MAP(CCSInceptApp)
	//}}AFX_MSG
	ON_COMMAND(ID_HELP, CWinApp::OnHelp)
END_MESSAGE_MAP()

/////////////////////////////////////////////////////////////////////////////
// CCSInceptApp construction

CCSInceptApp::CCSInceptApp()
{
}

/////////////////////////////////////////////////////////////////////////////
// The one and only CCSInceptApp object

CCSInceptApp theApp;

/////////////////////////////////////////////////////////////////////////////
// CCSInceptApp initialization

BOOL CCSInceptApp::InitInstance()
{
	// Standard initialization

#ifdef _AFXDLL
	Enable3dControls();			// Call this when using MFC in a shared DLL
#else
	Enable3dControlsStatic(); // Call this when linking to MFC statically
#endif

	CCSInceptDlg dlg;
	m_pMainWnd = &dlg;
	int nResponse = dlg.DoModal();
	if (nResponse == IDOK)
	{
	}
	else if (nResponse == IDCANCEL)
	{
```

```
        }

        // Since the dialog has been closed, return FALSE so that we exit the
        //  application, rather than start the application's message pump.
        return FALSE;
}
```

CSInceptDlg.cpp :

```
// CSInceptDlg.cpp : implementation file
//

#include "stdafx.h"
#include "CSIncept.h"
#include "CSInceptDlg.h"
#include "BdDlg.h"
#include "math.h"
#ifdef _DEBUG
#define new DEBUG_NEW
#undef THIS_FILE
static char THIS_FILE[] = __FILE__;
#endif

/////////////////////////////////////////////////////////////////////////////
// CAboutDlg dialog used for App About

class CAboutDlg : public CDialog
{
public:
	CAboutDlg();

// Dialog Data
	//{{AFX_DATA(CAboutDlg)
	enum { IDD = IDD_ABOUTBOX };
	//}}AFX_DATA

	// ClassWizard generated virtual function overrides
	//{{AFX_VIRTUAL(CAboutDlg)
	protected:
	virtual void DoDataExchange(CDataExchange* pDX);    // DDX/DDV support
	//}}AFX_VIRTUAL

// Implementation
protected:
	//{{AFX_MSG(CAboutDlg)
	//}}AFX_MSG
	DECLARE_MESSAGE_MAP()
};

CAboutDlg::CAboutDlg() : CDialog(CAboutDlg::IDD)
{
	//{{AFX_DATA_INIT(CAboutDlg)
	//}}AFX_DATA_INIT
}

void CAboutDlg::DoDataExchange(CDataExchange* pDX)
{
	CDialog::DoDataExchange(pDX);
	//{{AFX_DATA_MAP(CAboutDlg
	//}}AFX_DATA_MAP
}

BEGIN_MESSAGE_MAP(CAboutDlg, CDialog)
	//{{AFX_MSG_MAP(CAboutDlg)
```

```
            // No message handlers
        //}}AFX_MSG_MAP
END_MESSAGE_MAP()

/////////////////////////////////////////////////////////////////////////////
// CCSInceptDlg dialog

CCSInceptDlg::CCSInceptDlg(CWnd* pParent /*=NULL*/)
        : CDialog(CCSInceptDlg::IDD, pParent)
{
        //{{AFX_DATA_INIT(CCSInceptDlg)
        m_dvdt = 5000.0;
        m_d = 40.0;
        m_lp = 2.0;
        m_p = 300.0;
        m_rp = 0.3;
        //}}AFX_DATA_INIT
        m_hIcon = AfxGetApp()->LoadIcon(IDR_MAINFRAME);
}

void CCSInceptDlg::DoDataExchange(CDataExchange* pDX)
{
        CDialog::DoDataExchange(pDX);
        //{{AFX_DATA_MAP(CCSInceptDlg)
        DDX_Text(pDX, IDC_APPLIEDVOLTS, m_dvdt);
        DDX_Text(pDX, IDC_DISTANCE, m_d);
        DDX_Text(pDX, IDC_PARTLENGHT, m_lp);
        DDX_Text(pDX, IDC_PRESSURE, m_p);
        DDX_Text(pDX, IDC_TIPRADIUS, m_rp);
        //}}AFX_DATA_MAP
}

BEGIN_MESSAGE_MAP(CCSInceptDlg, CDialog)
        //{{AFX_MSG_MAP(CCSInceptDlg)
        ON_WM_SYSCOMMAND()
        ON_WM_PAINT()
        ON_WM_QUERYDRAGICON()
        ON_BN_CLICKED(IDOK, OnSIMULATE)
        //}}AFX_MSG_MAP
END_MESSAGE_MAP()

/////////////////////////////////////////////////////////////////////////////
// CCSInceptDlg message handlers

BOOL CCSInceptDlg::OnInitDialog()
{
        CDialog::OnInitDialog();

        // Add "About..." menu item to system menu.

        // IDM_ABOUTBOX must be in the system command range.
        ASSERT((IDM_ABOUTBOX & 0xFFF0) == IDM_ABOUTBOX);
        ASSERT(IDM_ABOUTBOX < 0xF000);

        CMenu* pSysMenu = GetSystemMenu(FALSE);
        CString strAboutMenu;
        strAboutMenu.LoadString(IDS_ABOUTBOX);
        if (!strAboutMenu.IsEmpty())
```

```
	{
		pSysMenu->AppendMenu(MF_SEPARATOR);
		pSysMenu->AppendMenu(MF_STRING, IDM_ABOUTBOX, strAboutMenu);
	}

	SetIcon(m_hIcon, TRUE);			// Set big icon
	SetIcon(m_hIcon, FALSE);		// Set small icon

	// TODO: Add extra initialization here

	return TRUE;  // return TRUE  unless you set the focus to a control
}

void CCSInceptDlg::OnSysCommand(UINT nID, LPARAM lParam)
{
	if ((nID & 0xFFF0) == IDM_ABOUTBOX)
	{
		CAboutDlg dlgAbout;
		dlgAbout.DoModal();
	}
	else
	{
		CDialog::OnSysCommand(nID, lParam);
	}
}

// If you add a minimize button to your dialog, you will need the code below
//  to draw the icon.  For MFC applications using the document/view model,
//  this is automatically done for you by the framework.

void CCSInceptDlg::OnPaint()
{
	if (IsIconic())
	{
		CPaintDC dc(this); // device context for painting

		SendMessage(WM_ICONERASEBKGND, (WPARAM) dc.GetSafeHdc(), 0);

		// Center icon in client rectangle
		int cxIcon = GetSystemMetrics(SM_CXICON);
		int cyIcon = GetSystemMetrics(SM_CYICON);
		CRect rect;
		GetClientRect(&rect);
		int x = (rect.Width() - cxIcon + 1) / 2;
		int y = (rect.Height() - cyIcon + 1) / 2;

		// Draw the icon
		dc.DrawIcon(x, y, m_hIcon);
	}
	else
	{
		CDialog::OnPaint();
	}
}

HCURSOR CCSInceptDlg::OnQueryDragIcon()
{
	return (HCURSOR) m_hIcon;
```

```
}

void CCSInceptDlg::OnSIMULATE()
{
        double uq=0, qcrit,f,q,t,g;
        double utip, ustream, uapplied, eback, lcorona, ldrift,tstep, etip;
        BOOL corona;
        double eps = 8.854e-12 ;
        double pi = 3.1415926535;
  CString str;

        CEdit* pEB1 = (CEdit*) GetDlgItem(IDC_DISTANCE);
        CEdit* pEB2 = (CEdit*) GetDlgItem(IDC_PARTLENGHT);
        CEdit* pEB3 = (CEdit*) GetDlgItem(IDC_TIPRADIUS);
        CEdit* pEB4 = (CEdit*) GetDlgItem(IDC_APPLIEDVOLTS);
        CEdit* pEB5 = (CEdit*) GetDlgItem(IDC_PRESSURE);
        pEB1->GetWindowText(str);
        m_d=atof((LPCTSTR)str);
        pEB2->GetWindowText(str);
        m_lp=atof((LPCTSTR)str);
        pEB3->GetWindowText(str);
        m_rp=atof((LPCTSTR)str);
        pEB4->GetWindowText(str);
        m_dvdt=atof((LPCTSTR)str);
        pEB5->GetWindowText(str);
        m_p=atof((LPCTSTR)str);

        m_d=m_d*1.0e-3;
        m_lp=m_lp*1e-3;
        m_rp=m_rp*1e-3;
        m_dvdt=m_dvdt*1e6;
        uq=0;
        m_p=m_p*1e3;
        f=0.1;
        tstep=0.1e-6;

        qcrit=45e-9*(pow((m_p/100e3),(-2.2)));
        q=0;
        t=0;
        utip=0;
        ustream=89*m_p*f*m_d;
        corona=0;

        t=t+tstep;
        uapplied=m_dvdt*t;
        utip=uapplied-uq;

        if (utip>ustream )
                corona =1;
        while (t<= 500e-6){
                if (corona){
                        eback = uapplied/m_d;
                        lcorona=0.5*(utip/(89*m_p));
                        ldrift=6*(eback/m_p)*tstep;
                        etip=(eback*(3+m_lp/(2*m_rp)));

                        q=((pi*eps*(pow((m_lp*etip),2)))/(89*m_p));
                        g=1/(2*(m_lp/(lcorona+ldrift)));
```

```
                uq=q/(g*pi*eps*m_lp);
                etip=(eback*(3+m_lp/(2*m_rp)))-(uq/(lcorona+ldrift));
                q=((pi*eps*(pow((m_lp*etip),2)))/(89*m_p));
                g=1/(2*(m_lp/(lcorona+ldrift)));
                uq=q/(g*pi*eps*m_lp);
        }
        if (q>= qcrit){
                CBdDlg dlg;
                dlg.m_v=uapplied;
                dlg.m_q=q;
                dlg.m_s=t;

                BOOL ret;
                ret=dlg.DoModal();

                break;
        }
        t=t+tstep;
        uapplied=m_dvdt*t;
        utip=uapplied-uq;
        if (utip>=ustream)
                corona=1;

    }

    AfxMessageBox("End of simulation");
}
```

BdDlg.cpp :

```
// BdDlg.cpp : implementation file
//

#include "stdafx.h"
#include "CSIncept.h"
#include "BdDlg.h"

#ifdef _DEBUG
#define new DEBUG_NEW
#undef THIS_FILE
static char THIS_FILE[] = __FILE__;
#endif

/////////////////////////////////////////////////////////////////////////////
// CBdDlg dialog


CBdDlg::CBdDlg(CWnd* pParent /*=NULL*/)
	: CDialog(CBdDlg::IDD, pParent)
{
	//{{AFX_DATA_INIT(CBdDlg)
	m_q = 0.0;
	m_s = 0.0;
	m_v = 0.0;
	//}}AFX_DATA_INIT
}


void CBdDlg::DoDataExchange(CDataExchange* pDX)
{
	CDialog::DoDataExchange(pDX);
	//{{AFX_DATA_MAP(CBdDlg)
	DDX_Text(pDX, IDC_CHARGE, m_q);
	DDX_Text(pDX, IDC_SECOND, m_s);
	DDX_Text(pDX, IDC_VOLT, m_v);
	//}}AFX_DATA_MAP
}


BEGIN_MESSAGE_MAP(CBdDlg, CDialog)
	//{{AFX_MSG_MAP(CBdDlg)
		// NOTE: the ClassWizard will add message map macros here
	//}}AFX_MSG_MAP
END_MESSAGE_MAP()

/////////////////////////////////////////////////////////////////////////////
// CBdDlg message handlers
```

StdAfx.cpp :

```
// stdafx.cpp : source file that includes just the standard includes
//        CSIncept.pch will be the pre-compiled header
//        stdafx.obj will contain the pre-compiled type information

#include "stdafx.h"
```

CSIncpet.h :

```
// CSIncept.h : main header file for the CSINCEPT application
//

#ifndef __AFXWIN_H__
        #error include 'stdafx.h' before including this file for PCH
#endif

#include "resource.h"            // main symbols

/////////////////////////////////////////////////////////////////////////////
// CCSInceptApp:
// See CSIncept.cpp for the implementation of this class
//

class CCSInceptApp : public CWinApp
{
public:
        CCSInceptApp();

// Overrides
        // ClassWizard generated virtual function overrides
        //{{AFX_VIRTUAL(CCSInceptApp)
        public:
        virtual BOOL InitInstance();
        //}}AFX_VIRTUAL

// Implementation

        //{{AFX_MSG(CCSInceptApp)
        //}}AFX_MSG
        DECLARE_MESSAGE_MAP()
};

/////////////////////////////////////////////////////////////////////////////
```

CSInceptDlg.h :

```
// CSInceptDlg.h : header file
//

/////////////////////////////////////////////////////////////////////////////
// CCSInceptDlg dialog

class CCSInceptDlg : public CDialog
{
// Construction
public:
	CCSInceptDlg(CWnd* pParent = NULL);	// standard constructor

// Dialog Data
	//{{AFX_DATA(CCSInceptDlg)
	enum { IDD = IDD_CSINCEPT_DIALOG };
	double	m_dvdt;
	double	m_d;
	double	m_lp;
	double	m_p;
	double	m_rp;
	//}}AFX_DATA

	// ClassWizard generated virtual function overrides
	//{{AFX_VIRTUAL(CCSInceptDlg)
	protected:
	virtual void DoDataExchange(CDataExchange* pDX);	// DDX/DDV support
	//}}AFX_VIRTUAL

// Implementation
protected:
	HICON m_hIcon;

	// Generated message map functions
	//{{AFX_MSG(CCSInceptDlg)
	virtual BOOL OnInitDialog();
	afx_msg void OnSysCommand(UINT nID, LPARAM lParam);
	afx_msg void OnPaint();
	afx_msg HCURSOR OnQueryDragIcon();
	afx_msg void OnSIMULATE();
	//}}AFX_MSG
	DECLARE_MESSAGE_MAP()
};
```

BdDlg.h :

```
// BdDlg.h : header file
//

/////////////////////////////////////////////////////////////////////////////
// CBdDlg dialog

class CBdDlg : public CDialog
{
// Construction
public:
	CBdDlg(CWnd* pParent = NULL);	// standard constructor

// Dialog Data
	//{{AFX_DATA(CBdDlg)
	enum { IDD = IDD_BDDLG };
	double	m_q;
	double	m_s;
	double	m_v;
	//}}AFX_DATA


// Overrides
	// ClassWizard generated virtual function overrides
	//{{AFX_VIRTUAL(CBdDlg)
	protected:
	virtual void DoDataExchange(CDataExchange* pDX);	// DDX/DDV support
	//}}AFX_VIRTUAL

// Implementation
protected:

	// Generated message map functions
	//{{AFX_MSG(CBdDlg)
		// NOTE: the ClassWizard will add member functions here
	//}}AFX_MSG
	DECLARE_MESSAGE_MAP()
};
```

StdAfx.h :

```
// stdafx.h : include file for standard system include files,
//  or project specific include files that are used frequently, but
//      are changed infrequently
//

#define VC_EXTRALEAN                    // Exclude rarely-used stuff from Windows headers

#include <afxwin.h>         // MFC core and standard components
#include <afxext.h>         // MFC extensions
#ifndef _AFX_NO_AFXCMN_SUPPORT
#include <afxcmn.h>                     // MFC support for Windows Common Controls
#endif // _AFX_NO_AFXCMN_SUPPORT
```

Resource.h :

```
//{{NO_DEPENDENCIES}}
// Used by CSIncept.rc
//
#define IDM_ABOUTBOX                    0x0010
#define IDD_ABOUTBOX                    100
#define IDS_ABOUTBOX                    101
#define IDD_CSINCEPT_DIALOG             102
#define IDR_MAINFRAME                   128
#define IDB_BITMAP1                     129
#define IDD_BDDLG                       130
#define IDC_DISTANCE                    1001
#define IDC_PARTLENGHT                  1002
#define IDC_VOLT                        1002
#define IDC_TIPRADIUS                   1003
#define IDC_SECOND                      1003
#define IDC_APPLIEDVOLTS                1004
#define IDC_CHARGE                      1004
#define IDC_PRESSURE                    1005

// Next default values for new objects
//
#ifdef APSTUDIO_INVOKED
#ifndef APSTUDIO_READONLY_SYMBOLS
#define _APS_NEXT_RESOURCE_VALUE        131
#define _APS_NEXT_COMMAND_VALUE         32771
#define _APS_NEXT_CONTROL_VALUE         1005
#define _APS_NEXT_SYMED_VALUE           101
#endif
#endif
```

CSIncept.mak :

```
# TARGTYPE "Win32 (x86) Application" 0x0101

!IF "$(CFG)" == ""
CFG=CSIncept - Win32 Debug
!MESSAGE No configuration specified.  Defaulting to CSIncept - Win32 Debug
!ENDIF

!IF "$(CFG)" != "CSIncept - Win32 Release" && "$(CFG)" !=\
 "CSIncept - Win32 Debug"
!MESSAGE Invalid configuration "$(CFG)" specified.
!MESSAGE You can specify a configuration when running NMAKE on this makefile
!MESSAGE by defining the macro CFG on the command line.  For example:
!MESSAGE
!MESSAGE NMAKE /f "CSIncept.mak" CFG="CSIncept - Win32 Debug"
!MESSAGE
!MESSAGE Possible choices for configuration are:
!MESSAGE
!MESSAGE "CSIncept - Win32 Release" (based on "Win32 (x86) Application")
!MESSAGE "CSIncept - Win32 Debug" (based on "Win32 (x86) Application")
!MESSAGE
!ERROR An invalid configuration is specified.
!ENDIF

!IF "$(OS)" == "Windows_NT"
NULL=
!ELSE
NULL=nul
!ENDIF
################################################################################
# Begin Project
# PROP Target_Last_Scanned "CSIncept - Win32 Debug"
RSC=rc.exe
MTL=mktyplib.exe
CPP=cl.exe

!IF "$(CFG)" == "CSIncept - Win32 Release"

# PROP BASE Use_MFC 6
# PROP BASE Use_Debug_Libraries 0
# PROP BASE Output_Dir "Release"
# PROP BASE Intermediate_Dir "Release"
# PROP BASE Target_Dir ""
# PROP Use_MFC 6
# PROP Use_Debug_Libraries 0
# PROP Output_Dir "Release"
# PROP Intermediate_Dir "Release"
# PROP Target_Dir ""
OUTDIR=.\Release
INTDIR=.\Release

ALL : "$(OUTDIR)\CSIncept.exe"

CLEAN :
```

```
	-@erase "$(INTDIR)\BdDlg.obj"
	-@erase "$(INTDIR)\CSIncept.obj"
	-@erase "$(INTDIR)\CSIncept.pch"
	-@erase "$(INTDIR)\CSIncept.res"
	-@erase "$(INTDIR)\CSInceptDlg.obj"
	-@erase "$(INTDIR)\StdAfx.obj"
	-@erase "$(OUTDIR)\CSIncept.exe"

"$(OUTDIR)" :
    if not exist "$(OUTDIR)/$(NULL)" mkdir "$(OUTDIR)"

# ADD BASE CPP /nologo /MD /W3 /GX /O2 /D "WIN32" /D "NDEBUG" /D "_WINDOWS" /D
"_AFXDLL" /D "_MBCS" /Yu"stdafx.h" /c
# ADD CPP /nologo /MD /W3 /GX /O2 /D "WIN32" /D "NDEBUG" /D "_WINDOWS" /D
"_AFXDLL" /D "_MBCS" /Yu"stdafx.h" /c
CPP_PROJ=/nologo /MD /W3 /GX /O2 /D "WIN32" /D "NDEBUG /D "_WINDOWS" /D\
 "_AFXDLL" /D "_MBCS" /Fp"$(INTDIR)/CSIncept.pch" /Yu"stdafx.h" /Fo"$(INTDIR)/"\
 /c
CPP_OBJS=.\Release/
CPP_SBRS=.\.
# ADD BASE MTL /nologo /D "NDEBUG" /win32
# ADD MTL /nologo /D "NDEBUG" /win32
MTL_PROJ=/nologo /D "NDEBUG" /win32
# ADD BASE RSC /l 0x409 /d "NDEBUG" /d "_AFXDLL"
# ADD RSC /l 0x409 /d "NDEBUG" /d "_AFXDLL"
RSC_PROJ=/l 0x409 /fo"$(INTDIR)/CSIncept.res" /d "NDEBUG" /d "_AFXDLL"
BSC32=bscmake.exe
# ADD BASE BSC32 /nologo
# ADD BSC32 /nologo
BSC32_FLAGS=/nologo /o"$(OUTDIR)/CSIncept.bsc"
BSC32_SBRS= \

LINK32=link.exe
# ADD BASE LINK32 /nologo /subsystem:windows /machine:I386
# ADD LINK32 /nologo /subsystem:windows /machine:I386
LINK32_FLAGS=/nologo /subsystem:windows /incremental:no\
 /pdb:"$(OUTDIR)/CSIncept.pdb" /machine:I386 /out:"$(OUTDIR)/CSIncept.exe"
LINK32_OBJS= \
	"$(INTDIR)\BdDlg.obj" \
	"$(INTDIR)\CSIncept.obj" \
	"$(INTDIR)\CSIncept.res" \
	"$(INTDIR)\CSInceptDlg.obj" \
	"$(INTDIR)\StdAfx.obj"

"$(OUTDIR)\CSIncept.exe" : "$(OUTDIR)" $(DEF_FILE) $(LINK32_OBJS)
    $(LINK32) @<<
  $(LINK32_FLAGS) $(LINK32_OBJS)
<<

!ELSEIF  "$(CFG)" == "CSIncept - Win32 Debug"

# PROP BASE Use_MFC 6
# PROP BASE Use_Debug_Libraries 1
# PROP BASE Output_Dir "Debug"
# PROP BASE Intermediate_Dir "Debug"
# PROP BASE Target_Dir ""
# PROP Use_MFC 6
# PROP Use_Debug_Libraries 1
```

```
# PROP Output_Dir "Debug"
# PROP Intermediate_Dir "Debug"
# PROP Target_Dir ""
OUTDIR=.\Debug
INTDIR=.\Debug

ALL : "$(OUTDIR)\CSIncept.exe"

CLEAN :
	-@erase "$(INTDIR)\BdDlg.obj"
	-@erase "$(INTDIR)\CSIncept.obj"
	-@erase "$(INTDIR)\CSIncept.pch"
	-@erase "$(INTDIR)\CSIncept.res"
	-@erase "$(INTDIR)\CSInceptDlg.obj"
	-@erase "$(INTDIR)\StdAfx.obj"
	-@erase "$(INTDIR)\vc40.idb"
	-@erase "$(INTDIR)\vc40.pdb"
	-@erase "$(OUTDIR)\CSIncept.exe"
	-@erase "$(OUTDIR)\CSIncept.ilk"
	-@erase "$(OUTDIR)\CSIncept.pdb"

"$(OUTDIR)" :
    if not exist "$(OUTDIR)/$(NULL)" mkdir "$(OUTDIR)"

# ADD BASE CPP /nologo /MDd /W3 /Gm /GX /Zi /Od /D "WIN32" /D "_DEBUG" /D
"_WINDOWS" /D "_AFXDLL" /D "_MBCS" /Yu"stdafx.h" /c
# ADD CPP /nologo /MDd /W3 /Gm /GX /Zi /Od /D "WIN32" /D "_DEBUG" /D "_WINDOWS" /D
"_AFXDLL" /D "_MBCS" /Yu"stdafx.h" /c
CPP_PROJ=/nologo /MDd /W3 /Gm /GX /Zi /Od /D "WIN32" /D "_DEBUG" /D "_WINDOWS"\
 /D "_AFXDLL" /D "_MBCS" /Fp"$(INTDIR)/CSIncept.pch" /Yu"stdafx.h"\
 /Fo"$(INTDIR)/" /Fd"$(INTDIR)/" /c
CPP_OBJS=.\Debug/
CPP_SBRS=.\.
# ADD BASE MTL /nologo /D "_DEBUG" /win32
# ADD MTL /nologo /D "_DEBUG" /win32
MTL_PROJ=/nologo /D "_DEBUG" /win32
# ADD BASE RSC /l 0x409 /d "_DEBUG" /d "_AFXDLL"
# ADD RSC /l 0x409 /d "_DEBUG" /d "_AFXDLL"
RSC_PROJ=/l 0x409 /fo"$(INTDIR)/CSIncept.res" /d "_DEBUG" /d "_AFXDLL"
BSC32=bscmake.exe
# ADD BASE BSC32 /nologo
# ADD BSC32 /nologo
BSC32_FLAGS=/nologo /o"$(OUTDIR)/CSIncept.bsc"
BSC32_SBRS= \

LINK32=link.exe
# ADD BASE LINK32 /nologo /subsystem:windows /debug /machine:I386
# ADD LINK32 /nologo /subsystem:windows /debug /machine:I386
LINK32_FLAGS=/nologo /subsystem:windows /incremental:yes\
 /pdb:"$(OUTDIR)/CSIncept.pdb" /debug /machine:I386\
 /out:"$(OUTDIR)/CSIncept.exe"
LINK32_OBJS= \
	"$(INTDIR)\BdDlg.obj" \
	"$(INTDIR)\CSIncept.obj" \
	"$(INTDIR)\CSIncept.res" \
	"$(INTDIR)\CSInceptDlg.obj" \
	"$(INTDIR)\StdAfx.obj"
```

```
"$(OUTDIR)\CSIncept.exe" : "$(OUTDIR)" $(DEF_FILE) $(LINK32_OBJS)
   $(LINK32) @<<
 $(LINK32_FLAGS) $(LINK32_OBJS)
<<

!ENDIF

.c{$(CPP_OBJS)}.obj:
  $(CPP) $(CPP_PROJ) $<

.cpp{$(CPP_OBJS)}.obj:
  $(CPP) $(CPP_PROJ) $<

.cxx{$(CPP_OBJS)}.obj:
  $(CPP) $(CPP_PROJ) $<

.c{$(CPP_SBRS)}.sbr:
  $(CPP) $(CPP_PROJ) $<

.cpp{$(CPP_SBRS)}.sbr:
  $(CPP) $(CPP_PROJ) $<

.cxx{$(CPP_SBRS)}.sbr:
  $(CPP) $(CPP_PROJ) $<

################################################################################
# Begin Target

# Name "CSIncept - Win32 Release"
# Name "CSIncept - Win32 Debug"

!IF  "$(CFG)" == "CSIncept - Win32 Release"

!ELSEIF  "$(CFG)" == "CSIncept - Win32 Debug"

!ENDIF

################################################################################
# Begin Source File

SOURCE=.\CSIncept.cpp
DEP_CPP_CSINC=\
	".\CSIncept.h"\
	".\CSInceptDlg.h"\
	".\StdAfx.h"\


"$(INTDIR)\CSIncept.obj" : $(SOURCE) $(DEP_CPP_CSINC) "$(INTDIR)"\
 "$(INTDIR)\CSIncept.pch"


# End Source File
################################################################################
# Begin Source File

SOURCE=.\CSInceptDlg.cpp
DEP_CPP_CSINCE=\
	".\BdDlg.h"\
```

```
	".\CSIncept.h"\
	".\CSInceptDlg.h"\
	".\StdAfx.h"\


"$(INTDIR)\CSInceptDlg.obj" : $(SOURCE) $(DEP_CPP_CSINCE) "$(INTDIR)"\
 "$(INTDIR)\CSIncept.pch"


# End Source File
################################################################################
# Begin Source File

SOURCE=.\StdAfx.cpp
DEP_CPP_STDAF=\
	".\StdAfx.h"\


!IF "$(CFG)" == "CSIncept - Win32 Release"

# ADD CPP /Yc"stdafx.h"

BuildCmds= \
	$(CPP) /nologo /MD /W3 /GX /O2 /D "WIN32" /D "NDEBUG" /D "_WINDOWS" /D\
 "_AFXDLL" /D "_MBCS" /Fp"$(INTDIR)/CSIncept.pch" /Yc"stdafx.h" /Fo"$(INTDIR)/"\
 /c $(SOURCE) \


"$(INTDIR)\StdAfx.obj" : $(SOURCE) $(DEP_CPP_STDAF) "$(INTDIR)"
   $(BuildCmds)

"$(INTDIR)\CSIncept.pch" : $(SOURCE) $(DEP_CPP_STDAF) "$(INTDIR)"
   $(BuildCmds)

!ELSEIF "$(CFG)" == "CSIncept - Win32 Debug"

# ADD CPP /Yc"stdafx.h"

BuildCmds= \
	$(CPP) /nologo /MDd /W3 /Gm /GX /Zi /Od /D "WIN32" /D "_DEBUG" /D "_WINDOWS"\
 /D "_AFXDLL" /D "_MBCS" /Fp"$(INTDIR)/CSIncept.pch" /Yc"stdafx.h"\
 /Fo"$(INTDIR)/" /Fd"$(INTDIR)/" /c $(SOURCE) \


"$(INTDIR)\StdAfx.obj" : $(SOURCE) $(DEP_CPP_STDAF) "$(INTDIR)"
   $(BuildCmds)

"$(INTDIR)\CSIncept.pch" : $(SOURCE) $(DEP_CPP_STDAF) "$(INTDIR)"
   $(BuildCmds)

!ENDIF

# End Source File
################################################################################
# Begin Source File

SOURCE=.\CSIncept.rc
DEP_RSC_CSINCEP=\
```

```
	".\res\bitmap1.bmp"\
	".\res\CSIncept.ico"\
	".\res\CSIncept.rc2"\


"$(INTDIR)\CSIncept.res" : $(SOURCE) $(DEP_RSC_CSINCEP) "$(INTDIR)"
  $(RSC) $(RSC_PROJ) $(SOURCE)


# End Source File
################################################################################
# Begin Source File

SOURCE=.\BdDlg.cpp
DEP_CPP_BDDLG=\
	".\BdDlg.h"\
	".\CSIncept.h"\
	".\StdAfx.h"\


"$(INTDIR)\BdDlg.obj" : $(SOURCE) $(DEP_CPP_BDDLG) "$(INTDIR)"\
 "$(INTDIR)\CSIncept.pch"


# End Source File
# End Target
# End Project
################################################################################
```

CSIncept.clw :

```
; CLW file contains information for the MFC ClassWizard

[General Info]
Version=1
LastClass=CBdDlg
LastTemplate=CDialog
NewFileInclude1=#include "stdafx.h"
NewFileInclude2=#include "CSIncept.h"

ClassCount=4
Class1=CCSInceptApp
Class2=CCSInceptDlg
Class3=CAboutDlg

ResourceCount=4
Resource1=IDD_ABOUTBOX
Resource2=IDR_MAINFRAME
Resource3=IDD_CSINCEPT_DIALOG
Class4=CBdDlg
Resource4=IDD_BDDLG

[CLS:CCSInceptApp]
Type=0
HeaderFile=CSIncept.h
ImplementationFile=CSIncept.cpp
Filter=N

[CLS:CCSInceptDlg]
Type=0
HeaderFile=CSInceptDlg.h
ImplementationFile=CSInceptDlg.cpp
Filter=D
BaseClass=CDialog
VirtualFilter=dWC
LastObject=CCSInceptDlg

[CLS:CAboutDlg]
Type=0
HeaderFile=CSInceptDlg.h
ImplementationFile=CSInceptDlg.cpp
Filter=D

[DLG:IDD_ABOUTBOX]
Type=1
Class=CAboutDlg
ControlCount=4
Control1=IDC_STATIC,static,1342177283
Control2=IDC_STATIC,static,1342308480
Control3=IDC_STATIC,static,1342308352
Control4=IDOK,button,1342373889

[DLG:IDD_CSINCEPT_DIALOG]
Type=1
Class=CCSInceptDlg
ControlCount=12
```

```
Control1=IDC_STATIC,static,1342177294
Control2=IDC_STATIC,static,1342308352
Control3=IDC_DISTANCE,edit,1350631552
Control4=IDC_STATIC,static,1342308352
Control5=IDC_PARTLENGHT,edit,1350631552
Control6=IDC_STATIC,static,1342308352
Control7=IDC_TIPRADIUS,edit,1350631552
Control8=IDC_STATIC,static,1342308352
Control9=IDC_APPLIEDVOLTS,edit,1350631552
Control10=IDC_STATIC,static,1342308352
Control11=IDC_PRESSURE,edit,1350631552
Control12=IDOK,button,1342242817

[DLG:IDD_BDDLG]
Type=1
Class=CBdDlg
ControlCount=11
Control1=IDOK,button,1342242817
Control2=IDC_STATIC,static,1342308352
Control3=IDC_STATIC,static,1342308352
Control4=IDC_STATIC,static,1342308352
Control5=IDC_STATIC,static,1342308352
Control6=IDC_STATIC,static,1342308352
Control7=IDC_VOLT,edit,1350633600
Control8=IDC_SECOND,edit,1350633600
Control9=IDC_CHARGE,edit,1350633600
Control10=IDC_STATIC,static,1342308352
Control11=IDC_STATIC,static,1342308352

[CLS:CBdDlg]
Type=0
HeaderFile=BdDlg.h
ImplementationFile=BdDlg.cpp
BaseClass=CDialog
Filter=D
VirtualFilter=dWC
LastObject=CBdDlg
```

CSIncept.rc :

```
// resource script
//
#include "resource.h"

#define APSTUDIO_READONLY_SYMBOLS
/////////////////////////////////////////////////////////////////////////////
//
// Generated from the TEXTINCLUDE 2 resource.
//
#include "afxres.h"

/////////////////////////////////////////////////////////////////////////////
#undef APSTUDIO_READONLY_SYMBOLS

/////////////////////////////////////////////////////////////////////////////
// English (U.S.) resources

#if !defined(AFX_RESOURCE_DLL) || defined(AFX_TARG_ENU)
#ifdef _WIN32
LANGUAGE LANG_ENGLISH, SUBLANG_ENGLISH_US
#pragma code_page(1252)
#endif //_WIN32

#ifdef APSTUDIO_INVOKED
/////////////////////////////////////////////////////////////////////////////
//
// TEXTINCLUDE
//

1 TEXTINCLUDE DISCARDABLE
BEGIN
    "resource.h\0"
END

2 TEXTINCLUDE DISCARDABLE
BEGIN
    "#include ""afxres.h""\r\n"
    "\0"
END

3 TEXTINCLUDE DISCARDABLE
BEGIN
    "#define _AFX_NO_SPLITTER_RESOURCES\r\n"
    "#define _AFX_NO_OLE_RESOURCES\r\n"
    "#define _AFX_NO_TRACKER_RESOURCES\r\n"
    "#define _AFX_NO_PROPERTY_RESOURCES\r\n"
    "\r\n"
    "#if !defined(AFX_RESOURCE_DLL) || defined(AFX_TARG_ENU)\r\n"
    "#ifdef _WIN32\r\n"
    "LANGUAGE 9, 1\r\n"
    "#pragma code_page(1252)\r\n"
    "#endif\r\n"
    "#include ""res\\CSIncept.rc2"" // non-Microsoft Visual C++ edited resources\r\n"
    "#include ""afxres.rc""     // Standard components\r\n"
```

```
  "#endif\0"
END

#endif   // APSTUDIO_INVOKED


/////////////////////////////////////////////////////////////////////////////
//
// Icon
//

// Icon with lowest ID value placed first to ensure application icon
// remains consistent on all systems.
IDR_MAINFRAME          ICON    DISCARDABLE     "res\\CSIncept.ico"

/////////////////////////////////////////////////////////////////////////////
//
// Dialog
//

IDD_ABOUTBOX DIALOG DISCARDABLE  0, 0, 217, 55
STYLE DS_MODALFRAME | WS_POPUP | WS_CAPTION | WS_SYSMENU
CAPTION "About CSIncept"
FONT 8, "MS Sans Serif"
BEGIN
    ICON            IDR_MAINFRAME,IDC_STATIC,11,17,20,20
    LTEXT           "CSIncept Version 1.0",IDC_STATIC,40,10,119,8,
                    SS_NOPREFIX
    LTEXT           "Copyright © 1997",IDC_STATIC,40,25,119,8
    DEFPUSHBUTTON   "OK",IDOK,178,7,32,14,WS_GROUP
END

IDD_CSINCEPT_DIALOG DIALOGEX 0, 0, 341, 182
STYLE DS_MODALFRAME | WS_POPUP | WS_VISIBLE | WS_CAPTION | WS_SYSMENU
EXSTYLE WS_EX_APPWINDOW
CAPTION "CSIncept"
FONT 8, "MS Sans Serif"
BEGIN
    CONTROL         129,IDC_STATIC,"Static",SS_BITMAP,129,7,44,30
    LTEXT           "Enter distance between plates (d) in mm :",IDC_STATIC,
                    73,54,122,8
    EDITTEXT        IDC_DISTANCE,200,53,99,12,ES_AUTOHSCROLL
    LTEXT           "Enter length of particle (Lp) in mm :",IDC_STATIC,93,71,
                    102,8
    EDITTEXT        IDC_PARTLENGHT,200,69,99,12,ES_AUTOHSCROLL
    LTEXT           "Enter radius of tip of particle in mm :",IDC_STATIC,90,
                    88,105,8
    EDITTEXT        IDC_TIPRADIUS,200,85,99,12,ES_AUTOHSCROLL
    LTEXT           "Enter rate of change of applied voltage in kV per microsecond :",
                    IDC_STATIC,8,105,187,8
    EDITTEXT        IDC_APPLIEDVOLTS,200,101,99,12,ES_AUTOHSCROLL
    LTEXT           "Enter pressure in kPascals :",IDC_STATIC,115,122,80,8
    EDITTEXT        IDC_PRESSURE,200,117,99,12,ES_AUTOHSCROLL
    DEFPUSHBUTTON   "SIMULATE",IDOK,145,161,50,14
END

IDD_BDDLG DIALOG DISCARDABLE  0, 0, 315, 126
STYLE DS_MODALFRAME | WS_POPUP | WS_CAPTION | WS_SYSMENU
```

```
CAPTION "Breakdown!"
FONT 8, "MS Sans Serif"
BEGIN
    DEFPUSHBUTTON   "OK",IDOK,131,105,50,14
    LTEXT           "Breakdown has occured.",IDC_STATIC,106,7,75,8
    LTEXT           "At a voltage of :",IDC_STATIC,17,28,47,8
    LTEXT           "in",IDC_STATIC,56,47,8,8
    LTEXT           "seconds",IDC_STATIC,251,48,31,8
    LTEXT           "at a charge of :",IDC_STATIC,19,66,45,8
    EDITTEXT        IDC_VOLT,69,25,177,15,ES_AUTOHSCROLL | ES_READONLY
    EDITTEXT        IDC_SECOND,69,46,177,13,ES_AUTOHSCROLL | ES_READONLY
    EDITTEXT        IDC_CHARGE,69,66,177,14,ES_AUTOHSCROLL | ES_READONLY
    LTEXT           "Volts",IDC_STATIC,252,28,16,8
    LTEXT           "Coulombs",IDC_STATIC,251,68,32,8
END


#ifndef _MAC
/////////////////////////////////////////////////////////////////////////////
//
// Version
//

VS_VERSION_INFO VERSIONINFO
 FILEVERSION 1,0,0,1
 PRODUCTVERSION 1,0,0,1
 FILEFLAGSMASK 0x3fL
#ifdef _DEBUG
 FILEFLAGS 0x1L
#else
 FILEFLAGS 0x0L
#endif
 FILEOS 0x4L
 FILETYPE 0x1L
 FILESUBTYPE 0x0L
BEGIN
    BLOCK "StringFileInfo"
    BEGIN
        BLOCK "040904B0"
        BEGIN
            VALUE "CompanyName", "\0"
            VALUE "FileDescription", "CSINCEPT MFC Application\0"
            VALUE "FileVersion", "1, 0, 0, 1\0"
            VALUE "InternalName", "CSINCEPT\0"
            VALUE "LegalCopyright", "Copyright © 1997\0"
            VALUE "LegalTrademarks", "\0"
            VALUE "OriginalFilename", "CSINCEPT.EXE\0"
            VALUE "ProductName", "CSINCEPT Application\0"
            VALUE "ProductVersion", "1, 0, 0, 1\0"
        END
    END
    BLOCK "VarFileInfo"
    BEGIN
        VALUE "Translation", 0x409, 1200
    END
END

#endif    // !_MAC
```

```
/////////////////////////////////////////////////////////////////////////////
//
// DESIGNINFO
//

#ifdef APSTUDIO_INVOKED
GUIDELINES DESIGNINFO DISCARDABLE
BEGIN
    IDD_ABOUTBOX, DIALOG
    BEGIN
        LEFTMARGIN, 7
        RIGHTMARGIN, 210
        TOPMARGIN, 7
        BOTTOMMARGIN, 48
    END

    IDD_CSINCEPT_DIALOG, DIALOG
    BEGIN
        LEFTMARGIN, 7
        RIGHTMARGIN, 334
        TOPMARGIN, 7
        BOTTOMMARGIN, 175
    END

    IDD_BDDLG, DIALOG
    BEGIN
        LEFTMARGIN, 7
        RIGHTMARGIN, 308
        TOPMARGIN, 7
        BOTTOMMARGIN, 119
    END
END
#endif    // APSTUDIO_INVOKED


/////////////////////////////////////////////////////////////////////////////
//
// Bitmap
//

IDB_BITMAP1             BITMAP  DISCARDABLE     "res\\bitmap1.bmp"

/////////////////////////////////////////////////////////////////////////////
//
// String Table
//

STRINGTABLE DISCARDABLE
BEGIN
    IDS_ABOUTBOX            "&About CSIncept..."
END

#endif    // English (U.S.) resources
/////////////////////////////////////////////////////////////////////////////



#ifndef APSTUDIO_INVOKED
```

```
/////////////////////////////////////////////////////////////////////////////
//
// Generate·' from the TEXTINCLUDE 3 resource.
/:
#define _AFX_NO_SPLITTER_RESOURCES
#define _AFX_NO_OLE_RESOURCES
#define _AFX_NO_TRACKER_RESOURCES
#define _AFX_NO_PROPERTY_RESOURCES

#if !defined(AFX_RESOURCE_DLL) || defined(AFX_TARG_ENU)
#ifdef _WIN32
LANGUAGE 9, 1
#pragma code_page(1252)
#endif
#include "res\CSIncept.rc2"  // non-Microsoft Visual C++ edited resources
#include "afxres.rc"         // Standard components
#endif
/////////////////////////////////////////////////////////////////////////////
#endif    // not APSTUDIO_INVOKED
```

References

1. Boeck I.W. *Twenty years of gas insulated substations- promises, problems and success of SF_6 application from 125kV up to 800kV+*, Elektron, March , pp.18-22, 1988.

2. Van Brunt R.J. , *Physics and Chemistry of Partial Discharge and Corona - Recent Advances and Future Challenges*, IEEE Transactions on Dielectrics and Electrical Insulation, Vol. 1, No.5 , pp. 761-784 , 1994.

3. Gallimberti I. , *A Computer Model For Streamer Propagation*, Journal of Physics D: Applied Physics, Vol. 5, pp. 2179-2188 , 1972.

4. Gallimberti I. And Bondiou A., *Theoretical Modelling of The Development Of The Positive Spark In Long Gaps*, Journal of Physics D: Applied Physics, Vol. 27, pp.1252-1266, 1994.

5. Wiegart, N. et al. *Research Report CEA No. 153 t 310 Corona stabilisation to testing of gas-insulating switchgear*, Canadian Electrical Association.

6. Arunachala Sastry K.S. et. al. , *Breakdown Of SF6 Gas Under Inhomogeneous Fields Under Impulse Voltage Of Different Waveshapes*, paper 32.01, Sixth International Symposium on High Voltage Engineering, New Orleans, 1989.

7. Wintle H.J. , *Basic Physics of Insulators*, IEEE Transactions on Electrical Insulation, Vol.25 , No.1 , pp.27-44 , 1990.

8. Van Der Zel, G.L. *Corona Stabilisation in SF6 and its influence on breakdown under fast rising impulses*. Ph.D. thesis, University Of The Witwatersrand, 1993.

9. Van Brunt R.J. , *Stochastic Properties of Partial Discharge Phenomena*, IEEE Transactions on Electrical Insulation, Vol.26 , No.5 , pp.902-948 ,1991.

10. Nicholson K., *Modelling Of Dynamical Systems*. Peter Peregrinus Ltd., 1980.

11. Van Der Zel G.L. and Reynders J.P. ,*Corona Stabilisation and its Influence on Breakdown Under Fast Rising Impulses* , paper 32-02, Seventh International Symposium on High Voltage Engineering, Dresden, 1991.

12. Kuffel E. and Zaengl W.S., *High Voltage Engineering Fundamentals*, Pergamon Press, 1984.

13. Gallimberti I. and Wiegart N. , *Streamer and Leader Formation in SF6 and SF6 Mixtures Under Positive Impulse Conditions: II. Streamer to Leader Transmission,* Journal of Physics D: Applied Physics, Vol. 19 , pp.2363-2379, 1986.

14. Gallimberti I. and Wiegart N. , *Streamer and Leader Formation in SF6 and SF6 Mixtures Under Positive Impulse Conditions: I. Corona Development,* Journal of Physics D: Applied Physics, Vol. 19 , pp.2351-2361, 1986.

15. Wiegart N. et al , *Inhomogenous Field Breakdown in GIS - The Prediction of Breakdown Probabilities and Voltages. Part I : Overview of a theory for inhomogeneous field breakdown in GIS* , IEEE Transactions on Power Delivery, Volume 3, No. 3, pp. 923-930, July 1988.

16. Wiegart N. et al , *Inhomogenous Field Breakdown in GIS - The Prediction of Breakdown Probabilities and Voltages. Part II : Ion Density and Statistical Time Lag* , IEEE Transactions on Power Delivery, Volume 3, No. 3, pp. 931-937, July 1988.

17. Niemeyer L. et al , *The Mechanism Of Leader Breakdown In Electronegative Gases,* IEEE Transactions on Electrical Insulation, Vol. 24, No.2 ,pp.309-324, 1989.

18. Pinnekamp F. and Niemeyer L. , *Leader Discharges In SF6,* Journal of Physics D: Applied Physics, Vol. 16, pp. 1031-1045, 1983.

19. Pinnekamp F. and Niemeyer L. , *Qualitative Model of Breakdown in SF6 in Inhomogenous Gaps* , Journal of Physics D: Applied Physics, Vol. 16, pp.1293-1302 , 1983.

20. Pinnekamp F. , *The Influence Of The Various Discharge Parameters On The Breakdown In Inhomogeneous SF6 Gaps* , 31-04 ,Fourth International Symposium on High Voltage Engineering, Athens, 1983.

21. Sigmond R. S. , *The Unipolar Space Charge Flow Problem* , Journal of Electrostatics, Vol. 18, pp. 249-272 , 1986.

22. Sigmond R. S. , *Simple Approximate Treatment Of Unipolar Space Charge Dominated Coronas : The Warburg Law and the Saturation Current* , Journal Of Applied Physics, Vol. 53, No.2, pp. 891-898, 1982.

23. Wintle H.J. , *Point-Plane and Edge-Plane Space Charge Limited Flows,* IEEE Transactions on Electrical Insulation, Vol.EI-21 , No.3 , pp.365-373,1986.

24. Wintle H.J. , *Space Charge Limited Current In The Needle-Plane Geometry,* Journal of Electrostatics, Vol.19 , pp. 257-274 , 1987.

25. Davies A.J. , *Discharge Simulation,* IEE Proceedings, Vol.133, Part A, no.4, pp. 217-240, 1986.

26. Date H. et al, *Analysis of the Electron Swarm Parameters by using Fourier Transforms of the Boltzmann Equation*, pp.844-847, Proceedings of the Tenth International Conference on Gas Discharges and their Applications, Swansea, 1992.

27. Morrow R. , *Theory of Positive Corona in SF6 Due To A Voltage Impulse.* IEEE Transactions On Plasma Science, Vol. 19, no. 2, pp.86-94, 1991.

28. Morrow R., *Theory Of Positive Onset Corona Pulses In SF6*, IEEE Transactions On Electrical Insulation, Vol. 26 , no. 3 , pp. 398-404 , 1991.

29. Morrow R. and Lowke J.J. , *Electrical Breakdown in Air and SF6*, Proceedings of the Fourth international conference on the Properties and Applications of Dielectric Materials, Paper No. 4248, Australia, 1994.

30. Morrow R. , *Properties Of Streamers And Streamer Channels In SF6*, Physical Review A, Vol. 35, no. 4, pp. 1778-1785, 1987.

31. Morrow R., *A Survey of the electron and ion transport properties of SF6*, IEEE Trans. On Plasma Science, Vol p5-14, no 3 ,pp. 234-239, 1986.

32. Morrow R. and Cram L.E. , *Flux-Corrected Transport and Diffusion on a Non-Uniform Mesh* , Journal of Computational Physics, Vol.57, pp.129-136, 1985.

33. Liu J. and Raju G.R.G. , *Streamer Formation and Monte Carlo Space-charge Field Calculation in SF6* , IEEE Transactions on Electrical Insulation, Vol.28 , No.2 , pp.261-270 , 1993.

34. Liu J. and Raju G.R.G. , *Simulation of Corona Discharge- Positive Corona in SF6* , IEEE Transactions on Dielectrics and Electrical Insulation, Vol.1 ,No.3 , pp.530-537 , 1994.

35. Liu J. and Raju G.R.G. , *Simulation of Corona Discharge- Negative Corona in SF6* , IEEE Transactions on Dielectrics and Electrical Insulation, Vol.1 ,No.3 , pp.520-529, 1994.

36. Peitgen H. et al, *Chaos and Fractals New Frontiers of Science,* Springer-Verlag, 1992.

37. Mandelbrot B.B. , *The Fractal Geometry of Nature*, Freeman, 1983.

38. Niemeyer et. al. , *Fractal Dimension Of dielectric Breakdown*, Physical Review Letters , Vol. 32, no. 12, pp.1033-1036, 1984.

39. Pietronero L. ,Wiesmann H.J. and Everstz C. , *Scaling Properties Of Growing Zone And Capacity Of Laplacian Fractals*, Proceedings of the Sixth Trieste International Symposium on Fractals in Physics, ICTP, Trieste, Italy, pp.159-163, 1985.

40. Wiesmann H.J. and Pietronero L. , *Properties Of Laplacian Fractals For Dielectric Breakdown In 2 and 3 Dimensions*, Fractals In Physics, Proceedings of the Sixth Trieste International Symposium on Fractals in Physics, ICTP, Trieste, Italy, pp.151-157, 1985.

41. Barclay et. al. , *Stochastic Modelling Of Electrical Treeing : Fractal And Statistical Characteristics*. Journal of Physics D: Applied Physics, Vol. 23, pp.536-545, 1990.

42. Egiziano L. et al , *Fractal Description of Electrical Discharges*, pp.137-144, Gaseous Dielectrics VI, Proceedings of the Sixth International Symposium on Gaseous Dielectrics, Knoxville, 1990.

43. Chatterton P.A. , *A Model For The Breakdown Of SF6 In The Presence Of Positive Impulse Corona*, paper 31.07, Third International Symposium on High Voltage Engineering, Milan . 1979.

44. Nitta T. and Shibuya Y. , *Electrical Breakdown of Long Gaps In Sulphur Hexafluoride*, IEEE Transactions on Power Apparatus and Systems, Vol. PAS 90, pp. 1065-1071, 1970.

45. Nelson J.K. et. al. , *Corona Stabilization In SF6/N2 Mixtures Under Impulse Conditions*, Proceedings Of The Third International Symposium On Gaseous Dielectrics, Knoxville, Tennessee, 1982

46. Abdel Salam M. et. al. , *Analysis of positive static corona-stabilised breakdown voltage of SF6, Part 1: Rising voltage-pressure characteristics* , Paper A78, IEEE PES Summer Meeting, Los Angeles, 1978.

47. Parekh H. And Srivastava K.D. , *Some Computations And Observations On Corona Stabilised Breakdown In SF6*. IEEE Transactions On Electrical Insulation, EI-15, Vol. 2 , 1980.

48. Parekh H. And Srivastava K.D. , *Effect Of Avalanche Space Charge Field On The Calculation Of Corona Onset Voltage*. IEEE Transactions On Electrical Insulation, Vol. EI-14, no. 4 , 1979.

49. Anis H. and Srivastava K.D. , *Pre-Breakdown Discharges in Rod Plane Gaps in SF6 Under Positive Switching Impulses*, IEEE Transactions on Electrical Insulation, Vol.EI-16 , No.6 , pp.552-563 , 1981.

50. Qiu, Y. et. Al. , *Effect of injected space charges on the positive impulse breakdown of SF6 in a point-plane gap* , Journal of Physics D: Applied Physics, Vol.25 , pp. 326-328, 1992.

51. Nelson, J.K. , *Modification of Corona Stabilisatio in Electronegative Gases by Low Ionization Potential Additives*, pp.175-183, Gaseous Dielectrics IV, Proceedings of the Fourth International Symposium on Gaseous Dielectrics, Knoxville, 1984.

52. Mufti A. H. et al, *Corona Characteristics for Free Conducting Particles In Various SF6 Gas Mixtures* , IEEE Transactions on Dielectrics and Electrical Insulation, Vol. 1, No. 3 ,pp. 509-519 , 1994.

53. Farish O. et al. , *The Streamer-Leader Transition In SF6 and SF6-Freon Mixtures*, 32-03, Sixth International Symposium on High Voltage Engineering, New Orleans, 1989.

54. Van Brunt R. J. And Misakian M. , *Mechanisms [illegible] nception Of D.C. And 60Hz A.C. Corona In SF6. IEEE Transactions On [illegible] cal Insulation*, Vol.EI-17, no.2, 1982.

55. Van Brunt R.J. and Leep D., *Characterization Of Point-Plane Corona Pulses in SF_6* ,J. Appl. Phys. , 52, p.6588, 1981.

56. Niemeyer L. et. al., *Phase Resolved Partial Discharge Mesurements In Particle Contaminated SF6 Insulation* pp.579-586, Gaseous Dielectrics VI, Proceedings of the Sixth International Symposium on Gaseous Dielectrics, Knoxville, 1990.

57. Farish O. et. al. , *Prebreakdown Corna Processes In SF6 And SF6 Mixtures*, paper 31.15, Third International Symposium on High Voltage Engineering, Milan., 1979.

58. Dale S.J. and Wooton R.E. , *Effect Of Fixed Particle Protrusions On 60Hz And Impulse Breakdown Voltage-Pressure Characteristics In SF6*, Paper 32.10, Third International Symposium on High Voltage Engineering, Milan , 1979.

59. Niemeyer L. , A Generalized Approach To Partial Discharge Modeling , IEEE Transactions on Dielectrics and Electrical Insulation, Vol.2, no.4, p.510, 1995.

60. Rong X. et al, *Influence Of The Steepness Of Impulse Voltages On The Corona Stabilization In SF_6* . Tenth International Conference On Gas Discharges And Their Applications, Swansea, p.238, 1992.

61. Cooke C.M., Surface Flashover Of Gas/Solid Interfaces, Third International Symposium on Gaseous Dielectrics, Knoxville, p.337, 1982.

62. Wiegart N. , *A Model for the production of initial electrons by detachment of SF_6 ions*, IEEE Transactions, Vol. 20, p.587, 1985.

63. Bhutt S. et al, *Preliminary Investigations of Positive-Impulse Corona in SF_6*, Proceedings of the Tenth International Symposium on High Voltage Engineering, Montreal, pp.363-366, 1997.

64. Hidaka K., *Progress in Japan of Space Charge Field Measurement in Gaseous Dielectrics Using a Pockels Sensor*, IEEE Electrical Insulation Magazine, Vol. 12, No.1, pp.17-28, 1996 .

65. Bhutt S. et al, *Corona Stabilisation In SF_6 : Current Understanding*, Proceedings of the Sixth South African Universities Power Engineering Conference, pp.9-12, 1996.

66. Bhutt S. et al, *Corona Stabilisation In SF_6 : Modelling*, Proceedings of the Sixth South African Universities Power Engineering Conference, pp.13-16,1996.

Bibliography

Amer R.Y. *Computation Of Positive Corona Onset Voltage For Compressed Gases.* Paper 32.12. 7'th International Symposium on High Voltage Engineering, Dresden, 1991.

Amer R.Y. *Breakdown Voltage Of SF6 At High Pressure.* Paper 32.13. 7'' International Symposium on High Voltage Engineering, Dresden, 1991.

Bartnikas R. and Novak J.P. , *On the Character of Different Forms of Partial Discharge and their Related Terminologies*, IEEE Transactions on Electrical Insulation, Vol.28 , No.6 , pp.956-967 , 1993

Berger G. et al. , *Time Lags In SF6 Under Impulse Conditions*, Proceedings Of The Third International Sympusium On Gaseous Dielectrics, Knoxville, Tennessee, 1982.

Boggs S.A. and Stone G.C. , *Fundamental Limitations In The Measurement Of Corona And Partial Discharge.* IEEE Transactions On Electrical Insulation, vol.EI-17 , no.2 , pp.143-145 , 1982

Boggs S.A., *Sulphur Hexafluoride - A complex dielectric*, IEEE Electrical Insulation Magazine, vol.6, no.1, 1990

Bohme H. , *Distribution Of The Breakdown-Voltage Of Gas-Insulation With Slightly Nonuniform Filed - A Model Concept.* Paper 32.15. 7'th International Symposium on High Voltage Engineering, Dresden, 1991.

Bouziane A. et. al. , *Assessment Of Corona Models Based On The Deutsch Approximation.* Journal of Physics D: Applied Physics, vol. 27, pp.320-329, 1994

Bouziane A. Et al, *Verification Of Direct-Current Corona Models Employing The Deutsch Approximation*, pp.407-412, Gaseous Dielectrics IV, Proceedings of the Sixth International Symposium on Gaseous Dielectrics, Knoxville, 1990

Chalmers I. D. et al, *Restrikes In SF6 Corona Channels - a Method of Channel Field Assessment* , Journal of Physics D: Applied Physics, Vol.22, pp. 1321-1326 , 1989

Cherukupalli S.E. et al , *Mechanism of Prebreakdown Spacer Charging in Nonuniform Fields under Unidirectional Voltages.* IEEE Transactions on Electrical Insulation, Vol.25 , No.4 , pp.642-654 , 1990

Danikas M.G. , *The Definitions Used for Partial Discharge Phenomena*, IEEE Transactions on Electrical Insulation, Vol.28 , No.6 , pp.1075-1081,1993

De Urquijo-Carmona J. et al, *Time-Resolved Study Of Charge Transfer In SF6*, Journal of Physics D: Applied Physics, Vol 19 , pp.L207-L210 , 1986

De Kok, N.J. *Redesign of computer model of breakdown in SF6 and development of computer model of partial discharges under impulse voltages.* M.Sc. thesis, The University Of The Witwatersrand, 1992.

Dincer M.S. and Aydin T. , *Simulation of Limiting Field Behaviour in Electron Swarms in SF6 N2 Gas Mixtures* , IEEE Transactions on Dielectrics and Electrical Insulation, Vol 1 , No. 1 ,pp 139-145 , 1994

Elmoursi A. A. and Speck C. E. , *Simulation of Space Charge in Unbounded Geometries*, IEEE Transactions on Industry Applications, Vol.26, N0.2, pp.384-392, 1990

Gilbert A. et. al. , *Dielectric Behaviour Of SF6 Point-Plane Gap Subjected To Fast Rising Impulse Voltage*, paper 25.04, 6'th International Symposium on High Voltage Engineering, New Orleans, 1989

Gleick J. *Chaos Making A New Science*, Penguin, 1987

Goldman M. and Goldman A. , *Corona Discharges*, Gaseous Electronics Vol 1 , editors Hirsh M.N. and Oskam H.J. , Academic Press Inc. , 1978. pp.219-285.

Goldman M. and Sigmond R.S. , *Corona and Insulation,* IEEE Transactions on Electrical Insulation, Vol.EI-17 , No.2 , pp. 90-105 , 1982

Hiesinger H. , *Leader Breakdown For Inhomogeneous Fields In Case Of VFT Conditions.* Paper 32.05. 7'th International Symposium on High Voltage Engineering, Dresden, 1991.

Hutzler B. , *Space Charges In Large Air Gaps* , 42-02 ,4'th International Symposium on High Voltage Engineering, Athens, 1983

Igarashi H. et al , *A Boundary Element Analysis of Space Charge Fields in a Corona Device* , IEEE Transactions On Magnetics, Vol. 29, No. 2, March 1993

Iwamoto M. et al. , *Analysis of Space Charge In Insulating Materials Under Non-Uniform Electric Fields.* IEEE Transactions on Electrical Insulation, Vol.EI-22 , No.4 , pp.419-424 , 1987

Jones J.E. And Davies M. , *A Critique Of The Deutsch Assumption*, Journal of Physics D: Applied Physics, vol. 25, pp.1749-1759, 1992

Khan M.M. and Nema R.S. , *Effect Of Surface Roughness On The Breakdown Phenomena In SF6 And Its Mixtures.* Paper 32.08. 7'th International Symposium on High Voltage Engineering, Dresden, 1991

Kuffel et. Al. , *Breakdown Of SF6 In Nonuniform Field Gaps Under Combined D.C. Fast Oscillating Impulse and Standard Lightning Impulse Voltages.* IEEE Transactions On Electrical Insulation, vol.28, no.2, 1993

Lakdawala V. K. , *Effect Of Ionization Processes On The Corona Stabilization Breakdown In SF6 and SF6-Mixtures,* 33-11 ,4'th International Symposium on High Voltage Engineering, Athens, 1983

Luxa G. et. Al. *Recent Research Activity On The Dielectric Performance Of SF6 With Special Reference To VFT s.* CIGRE Report , Vol 1, Paper 15-06, pp.106-120, 1988

Lyklema J.W. and Evertsz C. , *The Laplacian Random Walk,* Fractals In Physics, Proceedings of the Sixth Trieste International Symposium on Fractals in Physics, ICTP, Trieste, Italy, pp.87-92, 1985

Malik N.H. and Qureshi, *Breakdown Mechanisms In SF6,* IEEE Transactions on Electrical Insulation, Vol. EI-13 , No.3 , pp.135-145 , 1978

Mandelbrot B. B. , *An Overview Of The Language Of Fractals* , The Fractal Approach To Heterogeneous Chemistry, Avnir D. Ed. , John Wiley and Sons, 1989, pp. 3-9.

Matsumoto S. et.al. , *Non-uniform flashover mechanism in SF6 gas under fast-oscillating and non-oscillating impulse voltages,* paper 32.16, Sixth International Symposium on High Voltage Engineering, New Orleans, August/September 1989

Nema R. S. et. al. , *A Unified Approach For Calculation Of Breakdown Voltages Of Mixtures Of Electron-Attaching Gases.* Proceedings Of The Third International Symposium On Gaseous Dielectrics, Knoxville, Tennessee, 1982.

Niemeyer L. , *A Stepped Leader Random Walk Model.* Journal of Physics D: Applied Physics, Vol. 20 , pp.897-906, 1987

Ortega P. et. al. , *Predictive Modelling Of Positive Leader Propagation Under Standard And Oscillatory Impulse Shapes.* Journal of Physics D: Applied Physics, vol. 27, pp.1233-1241, 1994

Osamu Y. et al , *Behaviour Of Space Charge Produced By Positive Impulse Corona,* 41-04, 4'th International Symposium on High Voltage Engineering, Athens, 1983

Pedersen A. , *On The Electrical Breakdown Of Gaseous Dielectrics - An Engineering Approach*, IEEE Transactions on Electrical Insulation, Vol.24, No.5, pp.721-739 , 1989

Pedersen A. et al , *The Theory and Mesurement of Partial Discharge Transients,* IEEE Transactions on Electrical Insulation, Vol.26, No.3 , pp.487-497 , 1991

Pedersen A. , *Criteria For Spark Breakdown For Sulphur Hexafluoride*, IEEE Transactions on Power Apparatus and Systems, Vol. PAS-89, pp.2043-2048, 1970

Pfeifer P. And Obert M. , *Fractals : Basic Conce,.ts and Terminology,* The Fractal Approach To Heterogeneous Chemistry, Avnir D. Ed. , John Wiley and Sons, 1989, pp.11-43

Pfeiffer W. And Volker P. , *Formative Time Lag In SF6 and N2.* Proceedings Of The Third International Symposium On Gaseous Dielectrics, Knoxville, Tennessee, 1982.

Pfeiffer W. And Leitl A. , *About The Validity Of Sreamer Mechanism In Compressed Gases*, Proceedings Of The Third International Symposium On Gaseous Dielectrics, Knoxville, Tennessee, 1982.

Pompili M. et al, *The Effect of the Definition Used in Measuring Partial Discharge Inception Voltages* , IEEE Transactions on Electrical Insulation, Vol.28 , No.6 , pp.1002-1006 , 1993

Qiu Y. et. Al. , *Breakdown Of SF6 And Some SF6 Mixtures In A Point-Plane Sap*, Paper 32.09. 7'th International Symposium on High Voltage Engineering, Dresden, 1991.

Rusck S. , *SF6 Other Gases. Engineering Approach*, paper 32.00, Third International Symposium on High Voltage Engineering, Milan , 1979

Satpathy S. , *Dielectric Breakdown In Three Dimensions* , Proceedings of the Sixth Trieste International Symposium on Fractals in Physics, ICTP, Trieste, Italy, pp.173-176, 1985

Schmidt W.F. and Van Brunt R.J. , *Comments on The Effect Of Electron Detachment In Initiating Breakdown in Gaseous Dielectrics*, Proceedings Of The Third International Symposium On Gaseous Dielectrics, Knoxville, Tennessee, 1982.

Schmidt W.F. and Hilmert H. , *Electron Detachment From Negative Ions Of SF6 And Its Relation To Electric Breakdown.* Paper 32.06. 7'th International Symposium on High Voltage Engineering, Dresden, 1991.

Selim E.O. et al, *Space Charge Modelling in Impulse Corona*, 41-02, 4'th International Symposium on High Voltage Engineering, Athens, 1983

Somerville I.C. and Tedford D.J. , *The Statistical Time-Lag To Spark Breakdown In High Pressure SF6*, Proceedings Of The Third International Symposium On Gaseous Dielectrics, Knoxville, Tennessee, 1982.

Wetzer J.M. and Van Der Laan P.C.T. , *Prebreakdown Currents : Basic Interpretation And Time Resolved Measurements.* IEEE Transactions On Electrical Insulation, vol.24, no.2 , 1989

Wetzer J.M. and Van Der Laan P.C.T. , *Prebreakdown Currents Basic Interpretation and Time Resolved Measurements* , IEEE Transactions on Electrical Insulation, Vol.24 , No.2 , pp.297-308 , 1989

Yamamoto et. al. , *Behaviour Of Space Charge Produced By Positive Impulse Corona*. 4'th International Symposium on High Voltage Engineering, Athens, paper 41.04, 1983

Yu K. W. et al , *Computer Simulation Of Space Charge* , American Journal Of Physics, Vol. 59, No. 5, pp. 454-458, May 1991